https://doi.org/10.5194/amt-2019-496
Preprint. Discussion started: 6 February 2020

Atmospheric Measurement Techniques Discussions

The Airborne ROmanian Measurements of Aerosols and Trace gases (AROMAT) campaigns

Alexis Merlaud[1], Livio Belegante[2], Daniel-Eduard Constantin[3], Mirjam Den Hoed[4], Andreas Carlos Meier[5], Marc Allaart[4], Magdalena Ardelean[6], Maxim Arseni[3], Tim Bösch[5], Hugues Brenot[1], Andreea Calcan[6], Emmanuel Dekemper[1], Sebastian Donner[8], Steffen Dörner[8], Carmelia Dragomir[3], Lucian Georgescu[3], Anca Nemuc[2], Doina Nicolae[2], Gaia Pinardi[1], Andreas Richter[5], Adrian Rosu[3], Thomas Ruhtz[7], Anja Schönhardt[5], Dirk Schuettemeyer[10], Reza Shaiganfar[8], Kerstin Stebel[9], Frederik Tack[1], Sorin Nicolae Vâjâiac[6], Jeni Vasilescu[2], Jurgen Vanhamel[1], Thomas Wagner[8], and Michel Van Roozendael[1]

[1]Royal Belgian Institute for Space Aeronomie (BIRA-IASB), Avenue Circulaire 3, 1180 Brussels, Belgium
[2]National Institute of R&D for Optoelectronics (INOE), Magurele, Street Atomistilor 409, Magurele 77125, Romania
[3]"Dunarea de Jos" University of Galati, Faculty of Sciences and Environment, Str. Domneasca, Nr. 111, Galati 800008, Romania
[4]Royal Netherlands Meteorological Institute (KNMI), De Bilt, The Netherlands
[5]Institute of Environmental Physics, University of Bremen (IUP-Bremen), Otto-Hahn-Allee 1, 28359 Bremen, Germany
[6]National Institute for Aerospace Research "Elie Carafoli" (INCAS), Bd. Iuliu Maniu no. 220, Bucharest, Romania
[7]Institute for Space Sciences, Free University of Berlin (FUB), Carl-Heinrich-Becker-Weg 6-10, 12165 Berlin, Germany
[8]Max-Planck-Institute for Chemistry (MPIC), Hahn-Meitner-Weg 1, 55128 Mainz, Germany
[9]Norwegian Institute for Air Research (NILU), Instituttveien 18, 2007 Kjeller, Norway
[10]European Space Agency (ESA-ESTEC), Keplerlaan 1, 2201 AZ Noordwijk, The Netherlands

Correspondence: A.Merlaud (alexism@oma.be)

Abstract.

The Airborne ROmanian Measurements of Aerosols and Trace gases (AROMAT) campaigns took place in Romania in September 2014 and August 2015. They focused on two sites: the Bucharest urban area and the power plants in the Jiu Valley. Their main objectives were to test recently developed airborne observation systems dedicated to air quality studies and to verify the concept of such campaigns in support of the validation of spaceborne atmospheric missions such as the TROPOspheric Monitoring Instrument (TROPOMI)/Sentinel-5 Precursor (S5P).

We show that tropospheric NO_2 vertical column density (VCD) measurements using airborne mapping instruments are in principle valuable for satellite validation. The signal to noise ratio of the airborne NO_2 measurements is one order of magnitude higher than its spaceborne counterpart when the airborne measurements are averaged at the TROPOMI pixel scale. A significant source of comparison error appears to be the time variation of the NO_2 VCDs during a flight, which we estimated at about 4x10^{15} molec cm^{-2} in the AROMAT conditions. Considering the random error of the TROPOMI tropospheric NO_2 VCD (σ), the dynamic range of the NO_2 VCDs field extends from detection limit up to 37 σ (2.6x10^{16} molec cm^{-2}) or 29 σ (2x10^{16} molec cm^{-2}) for Bucharest and the Jiu Valley, respectively. For the two areas, we simulate validation exercises of the TROPOMI tropospheric NO_2 product using airborne measurements. These simulations indicate that we can closely approach the TROPOMI optimal target accuracy of 25% by adding NO_2 and aerosol profile information to the airborne mapping obser-

https://doi.org/10.5194/amt-2019-496
Preprint. Discussion started: 6 February 2020


Atmospheric Measurement Techniques Discussions

vations, which constrains the investigated accuracy to within 28%. In addition to NO_2, we also measured significant amounts of SO_2 in the Jiu Valley, as well as a hotspot of H_2CO in the center of Bucharest. For these two species, we conclude that the best validation strategy would consist in deploying ground-based measurement systems at key locations which the AROMAT observations help identify.

1 Introduction

Since the launch of the Global Ozone Monitoring Experiment (GOME, Burrows et al. (1999)) in 1995, spaceborne observations of reactive gases in the UV-visible range have tremendously improved our understanding of tropospheric chemistry. GOME mapped the large urban sources of NO_2 in North America and Europe, the SO_2 emissions from volcanoes and coal-fired power plants (Eisinger and Burrows, 1998), and the global distribution of H_2CO with its maxima above East Asia and the tropical forests (De Smedt et al., 2008). Subsequent air-quality satellite missions expanded on the observation capabilities of GOME. Table 1 lists the past, present, and near-future nadir-looking satellite instruments dedicated to ozone and air quality monitoring with their sampling characteristics in space and time. The pixel size at nadir has shrunk from 320x40 km^2 (GOME) to 3.5x5.5 km^2 (TROPOMI, Veefkind et al. (2012)). This high horizontal resolution enables for instance to disentangle contradictory trends in ship and continental emissions of NO_2 in Europe (Boersma et al., 2015) or to distinguish the different NO_2 sources in oil sand mines in Canada (Griffin et al., 2019). The satellite-derived air quality products are now reliable enough to improve the bottom-up emission inventories (e.g. Kim et al. (2009), Fioletov et al. (2017), Bauwens et al. (2016)) and to be used in operational services, for instance to assist air traffic control with the near-real time detection of volcanic eruptions (Brenot et al., 2014). The bottom lines of Table 1 presents the near-future perspective in spaceborne observation of the troposphere: a constellation of geostationary satellites will provide hourly observations of the troposphere above east Asia (GEMS, (Kim, 2012)), North America (TEMPO, Chance et al. (2013)), and Europe (Sentinel-4, Ingmann et al. (2012)). These new developments will open-up new perspectives for atmospheric research and air quality policies (Judd et al., 2018).

Validation is a key aspect of any spaceborne Earth observation mission. This aspect becomes even more important as the science matures and leads to more operational and quantitative applications. Validation involves a statistical analysis of the differences between measurements to be validated and reference measurements (von Clarmann, 2006). The aim of validation is to verify that the satellite data products meet their requirements in terms of accuracy and precision. Table 2 presents such requirements for the TROPOMI-derived tropospheric vertical column densities (VCDs) of NO_2, SO_2, and H_2CO (ESA, 2014). Richter et al. (2014) have discussed the challenges associated with the validation of tropospheric reactive gases. These challenges arise from the large variability in space and time of short-lived reactive gases, the dependency of the satellite products on different geophysical parameters (surface albedo, profile of trace gases and aerosols), the differences in vertical sensitivity between satellite and reference (ground-based or airborne) measurements, and the small signals. An ideal validation study would involve a reference dataset of VCDs whose well-characterized uncertainties would be small compared to those required for the investigated products. This reference dataset would cover a large amount of satellite pixels with adequate spatial and temporal representativeness at different seasons, places, and pollution levels. Beside the VCDs, the ideal validation exercise

https://doi.org/10.5194/amt-2019-496
Preprint. Discussion started: 6 February 2020


Atmospheric Measurement Techniques Discussions

would also quantify the geophysical parameters that impact the retrieval of the investigated satellite products. In the real world however, Richter et al. points out that "the typical validation measurement falls short in one or even many of these aspects".

The first validations of the tropospheric NO_2 and H_2CO VCD products of GOME involved in-situ samplings from aircraft (Heland et al., 2002; Martin et al., 2004). Such measurements may cover good fractions of satellite pixels but they miss the lower part of the boundary layer, where the trace gas concentrations often peak. Schaub et al. (2006) and Boersma et al. (2011) summarize other early validation studies for the tropospheric NO_2 VCDs retrieved from GOME, SCIAMACHY, and OMI. Several of these studies make use of the NO_2 surface concentration datasets from air quality monitoring networks. Compared to campaign-based data acquisition, operational in-situ networks provide long-term measurements, but their comparison with satellite products relies upon assumptions on the NO_2 profile. Other validation studies use remote-sensing from the ground and aircraft, in particular based on the Differential Optical Absorption Spectroscopy (DOAS) technique (Platt and Stutz, 2008), which is also the basis for the retrieval algorithms of the satellite-derived products. In comparison with in-situ measurements, DOAS has the benefit of being directly sensitive to the column density of a trace gas, i.e. the same geophysical quantity which is retrieved from space. Heue et al. (2005) conducted the first comparison between a satellite-derived product (SCIAMACHY tropospheric NO_2) and airborne DOAS data. Many validation studies also use ground-based DOAS measurements, in particular since the development of the Multi-AXis DOAS (MAX-DOAS) technique (Hönninger et al., 2004). MAX-DOAS measurements are valuable for validation due to their ability to measure integrated columns at spatial scales comparable to the satellite ground pixel size. Moreover, they broaden the scope of validation activities since they also provide limited profile information on both trace gases and aerosols (Irie et al., 2008; Brinksma et al., 2008; Ma et al., 2013; Kanaya et al., 2014; Wang et al., 2017; Drosoglou et al., 2018). The limitations of using the MAX-DOAS technique for validation arise from their still imperfect spatial representativeness compared to typical satellite footprints and to some extent from their limited sensitivity in the free troposphere. Spatial representativeness has often been invoked to explain the apparent low bias of the OMI tropospheric NO_2 VCDs in urban conditions (Boersma et al., 2018).

The unprecedented horizontal resolution enabled by the last generation of air-quality space-based instruments motivated preparatory field studies around polluted areas in North America (DISCOVER-AQ, https://discover-aq.larc.nasa.gov), Europe (AROMAT and AROMAPEX, Tack et al.,2019) and Korea (KORUS-AQ, https://www-air.larc.nasa.gov/missions/korus-aq/). These campaign activities quantified key pollutants (NO_2, SO_2, O_3, H_2CO, and aerosols) and assessed practical observation capabilities of future satellite instruments while preparing for their validation. They combined ground-based and airborne measurements. DISCOVER-AQ involved the deployment of the Geostationary Trace gas and Aerosol Sensor Optimization instrument (GEOTASO, Leitch et al.,2014; Nowlan et al.,2016) and of the Geostationary Coastal and Air Pollution Events (GEO-CAPE) Airborne Simulator (GCAS, Kowalewski and Janz,2014;Nowlan et al.,2018). In Europe, the two AROMAT campaigns, which took place in Romania in September 2014 and August 2015, demonstrated a suite of new instruments such as the Airborne imaging DOAS instrument for Measurements of Atmospheric Pollution (AirMAP, Schönhardt et al.,2015; Meier et al.,2017), the NO_2 sonde (Sluis et al., 2010), and the Small Whiskbroom Imager for atmospheric compositioN monitorinG (SWING, Merlaud et al.,2018). Different airborne imagers were intercompared and further characterized during the AROMAPEX campaign in April 2016 (Tack et al., 2019).

https://doi.org/10.5194/amt-2019-496
Preprint. Discussion started: 6 February 2020


Atmospheric Measurement Techniques Discussions

In this work, we introduce the measurements performed during the AROMAT campaigns and analyze their relevance for the validation of air quality satellite products. The datasets collected during AROMAT fulfill several requirements of the ideal validation study, as described above. We further investigate the strengths and limitations of the acquired data sets.

The paper is structured as follows: Section 2 describes the two target areas and the deployment strategy. Section 3 characterizes the geophysical fields of the sampled areas and Section 4 presents a critical analysis of the strengths and limitations of the campaign results while elaborating on recommendations for future validation campaigns in Romania. The supplement lists the main instruments operated during the campaigns, gives practical details about their deployment, and presents additional information and measurements.

2 Target areas and deployment strategy

This section presents the two target areas of the AROMAT campaigns, Bucharest and the Jiu Valley. It also lists available studies on air quality at these two sites as well as logistical aspects of relevance.

Figure 1 presents a map of the tropospheric NO_2 vertical column densities (VCDs) above Romania, derived from OMI measurements (Levelt et al., 2006) and averaged between 2012 and 2016. The map also indicates the position of the 8 largest cities of the country. Compared to highly polluted areas in western Europe such as northern Belgium or the Netherlands, Romania appears relatively clean at the spatial resolution of the satellite data. There are however two major NO_2 sources clearly visible from space, which appear to be of similar magnitude with NO_2 columns around 2.5 x 10^{15} molec cm^{-2}: the Bucharest area and the Jiu Valley, northwest of Craiova. For the latter, the NO_2 enhancement is due to a series of large coal-fired thermal power plants.

2.1 Bucharest

Bucharest (44.4° N, 26.1° E) is the capital and largest city (1.9 million inhabitants according to the 2011 census) of Romania. Within its administrative borders, the city covers an area of 228 km^2. Adding the surrounding Ilfov county, the total Bucharest metropolitan area numbers 2.3 million inhabitants in 1.583 km^2. The built-up areas are mainly located within a ring road whose diameter is around 20 km.

lorga et al. (2015) described in detail the Bucharest Greater Area in the context of an extensive study of the air quality in the city between 2005 and 2010. Bucharest is located in a low-altitude plain, with a maximum altitude of 92 m a.s.l. The geographic configuration of the Carpathian Mountains explains the dominant northeast winds.

The NO_2 VCDs seen from space above Bucharest appear lower than over western European sites at the resolution of OMI (see Fig.S7 in the Supplement). However, this is partly due to the dilution effect for this relatively small and isolated source. Local studies based on the 8 air quality stations inside the city point out that, regarding local PM and NO_x levels, Bucharest is amongst the most polluted cities in Europe (Alpopi and Colesca, 2010; lorga et al., 2015). The city center is the most heavily polluted, with concentrations of pollutants well above the European thresholds. For instance, the annual mean concentration of NO_2 at the traffic stations was about 57 μ g.m^{-3} in 2017 (EEA, 2019). Stefan et al. (2013) have shown the importance of local

https://doi.org/10.5194/amt-2019-496
Preprint. Discussion started: 6 February 2020


Atmospheric Measurement Techniques Discussions

conditions and anthropogenic factors in air quality analysis in areas close to Bucharest, during two weeks of measurements in 2012. Iorga et al. (2015) and Grigoraş et al. (2016) showed that the main NO_x contributions came from traffic and production of electricity, spread over about 10 medium-size thermal power plants within the city.

Figure 2 shows the Bucharest metropolitan area and the flight tracks of the two scientific aircraft used during AROMAT-2 (the FUB Cessna-207 and the INCAS BN-2). Note that the BN-2 tracks are actually a good indication of the Bucharest ring road. We were not allowed to cross the ring road with the BN-2, except in the North of the city. The figure also pinpoints important locations for the AROMAT campaigns. The FUB Cessna took-off and landed at the Baneasa international airport, located 8 km north of Bucharest city center (44.502° N, 26.101° E). The INCAS BN-2 also used Baneasa airport during AROMAT-2, but this plane was mainly based at the Strejnicu airfield (44.924° N, 25.964° E), which lies 60 km north of Bucharest, near Ploiesti. The UAV operations in Bucharest during AROMAT-1 were performed at Clinceni airfield (44.359° N, 25.931 ° E). The latter is located in the southwest of the city, 7 km west of the INOE observatory in Magurele (44.348°N, 26.031°E).

2.2 The Jiu Valley between Targu Jiu and Craiova

The second NO_2 plume in Fig. 1 lies around 250 km west of Bucharest. It corresponds to a series of four thermal power plants located along the Jiu river between the cities of Targu Jiu (82,000 inhabitants, 45.03°N, 23.27°E) and Craiova (269,000 inhabitants, 44.31°N, 23.8°E). These plants were built in this area due to the presence of lignite (brown coal), which is burned to produce electricity.

The altitude of the valley ranges from 268 m a.s.l. in Targu Jiu to 90 m in Craiova. The valley is surrounded by moderately elevated hills (400 m a.s.l.). Due to the orography, the prevailing wind directions is from southwest to southeast.

Beside NO_2, the SO_2 emissions from these plants are also visible from space, as first reported by Eisinger and Burrows (1998) using GOME data. Since 2011, the OMI-derived trends above the area indicate that the emissions of SO_2 have been decreasing, while those of NO_2 are stable (Krotkov et al., 2016). This is related to the installation of flue gas desulfurization (FGD) systems, which was part of environmental regulations imposed on Romania following its entry in the European Union in 2007.

Figure 3 presents a map of the Jiu Valley area with the four power plants. The map also shows the tracks of the two airborne platforms (the FUB Cessna and an ultralight operated by UGAL) operated in this area during AROMAT-2. Table 3 presents the geographical positions, nominal capacities, and smokestack heights of the four power plants. From north to south, the plants are named according to their locations: Rovinari, Turceni, Isalnita and Craiova II.

During the AROMAT campaigns, we focused in particular on the emissions of the Turceni power plant (44.67°N, 23.41°E). With a nominal capacity of 1650 MW, it is the largest electricity producer in Romania. The Turceni power plant is located in a rural area, 2 km ESE of the village of Turceni. The plant emits aerosols, NOx, and SO_2 from the 280 m high smokestacks.

Scientific studies on air quality inside the Jiu Valley are sparse. Previous measurements performed by INOE during a campaign in Rovinari in 2010 indicated elevated volume mixing ratios of NO_2 (up to 30 ppb) and of SO_2 (up to 213 ppb) (Nisulescu et al., 2011; Marmureanu et al., 2013). The maximum ground concentrations occurred in the morning, before the planetary

https://doi.org/10.5194/amt-2019-496
Preprint. Discussion started: 6 February 2020


Atmospheric Measurement Techniques Discussions

boundary layer development. Mobile-DOAS observations performed in 2013 revealed columns of NO_2 up to 1 x 10^{17} molec cm^{-2} (Constantin et al., 2015).

2.3 Groups, instruments, and platforms

The AROMAT consortium consisted of research teams from Belgium (BIRA-IASB), Germany (IUP-Bremen, FUB, MPIC), The Netherlands (KNMI), Romania (University "Dunarea de Jos" of Galati, hereafter UGAL, National Institute of R&D for Optoelectronics, hereafter INOE, and National Institute for Aerospace Research "Elie Carafoli", hereafter INCAS), and Norway (NILU). The AROMAT consortium had a common focus on measuring the tropospheric composition using various techniques.

The supplement presents the main atmospheric instruments operated during the two campaigns, classified into airborne, ground-based, remote sensing, and in-situ sensors. The primary target species during AROMAT-1 were NO_2 and aerosols while the observation capacities expanded in AROMAT-2 through the improvements of the AirMAP and SWING sensors for SO_2 measurements and the deployments of other instruments such as SO_2 cameras, DOAS instruments targeted to H_2CO, and a PICARRO instrument to measure water vapor, methane, CO, and CO_2.

We used two small tropospheric aircraft: the Cessna-207 from FUB, and the Britten-Norman Islander (BN-2) from INCAS. The Cessna was dedicated to remote sensing. It mainly performed mapping flights at 3 km a.s.l. for the airborne imagers, while parts of the ascents and descents were used to measure aerosol extinction profiles with the FUBISS-ASA2 instrument. The BN-2, which was only used during AROMAT-2, was dedicated to in-situ measurements around Bucharest between surface and 3000 m a.s.l.. In AROMAT-2, there was also an ultralight aircraft used by UGAL for nadir-DOAS observations in the Jiu Valley. The ultralight aircraft typically flew between 600 and 1800 m a.s.l. Two UAVs, operated by INCAS and UGAL flew during AROMAT-1. These measurements were not repeated during AROMAT-2 since the coverage of the UAVs was too limited, both in horizontal and vertical direction. Finally, we also launched balloons carrying NO_2 sondes from Turceni and performed Mobile-DOAS measurements from several cars during both campaigns. The supplement provides more details about the practical deployments during the campaigns.

3 Geophysical results

This section presents selected findings related to the atmospheric structure and the geophysical fields of trace gases and aerosols in the two target areas. The Supplement gives details of the instruments involved in these observations. Tables S6 and S7 of the Supplement summarize the observed ranges of the main geophysical quantities for the two campaigns.

3.1 Bucharest

3.1.1 Aerosol optical properties

Figure 4 shows the lidar extinction profiles at 532 nm measured at INOE in Margurele (44.35° N, 26.03° E) during two days of AROMAT-2: 30 (red), and 31 (blue) August 2015. We retrieved these daytime extinction profiles from the backscatter profiles

https://doi.org/10.5194/amt-2019-496
Preprint. Discussion started: 6 February 2020


Atmospheric Measurement Techniques Discussions

using a column-averaged lidar ratio constrained with the AOD from collocated sunphotometer measurements. The extinction was larger on 30 August 2015. It reached 0.21 km^{-1} in the boundary layer and up to 0.32 km^{-1} in an elevated layer at 2 km altitude. A similar elevated layer also appeared in the FUBISS data (Meier et al., 2017, Fig.7).

During AROMAT-2, the AOD at 532 nm was around 0.2 most of the days, except on 30 August 2015 (0.35) and 1 September 2015 (0.05). Interestingly, the maximum AOD was seen on a Sunday, when the anthropogenic emissions of NO_x from Bucharest were minimal, as indicated by Fig. 7, which compares the NO_2 above the city on Sunday 30 August and Monday 31 August 2015.

3.1.2 Boundary layer height

We estimated the boundary layer height (BLH) using a gradient method applied to the lidar range corrected signal (Belegante et al., 2014; Timofte et al., 2015). Figure 5 presents such BLH estimates using the RALI lidar observations during AROMAT-2 in Bucharest. The BLH varied between 700 m (morning of the 30 August 2015) and 2500 m (afternoon of the 24, 26, and 31 August 2015). During AROMAT-1, similar estimates resulted in BLH ranging between 1300 m (2 September 2014) and 2200 m (11 September 2014).

Figure 6 presents the PICARRO measurements of CO, CH_4, H_2O, and CO_2 volume mixing ratios (vmr) during two soundings of the BN-2: (i) between 11:24 and 11:41 UTC on 30 August 2015 (ii) between 12:20 and 12:39 UTC on 31 August 2015. All the species exhibit clear discontinuities in their vertical distribution at the altitude of the lidar-derived BLH: 800 m on 30 August 2015 and 1200 m a.s.l on 31 August 2015.

Except for CH_4 on 31 August 2015, the vmrs were relatively stable in the boundary layer, and rapidly decreased above. Both soundings exhibit more polluted layers aloft, probably linked with long-range transport. These vertical distributions give confidence in the lidar-derived BLH, under which convection and turbulences homogenize the distribution of aerosols and trace gases.

Unfortunately, the BN-2 did not vertically sample the exhaust plume of Bucharest due to flight restrictions. We thus have little access to the vertical distributions of the aerosols and NO_2 in the Bucharest plume.

3.1.3 Horizontal distribution of NO_2

Figure 7 presents two maps of the AROMAT NO_2 measurements performed with the AirMAP, CAPS, and MPIC mobile-DOAS instruments above Bucharest, on 30 (Sunday afternoon, left panel) and 31 (Monday afternoon, right panel) August 2015. AirMAP is a remote sensing instrument that mapped the NO_2 VCDs from the Cessna at 3 km a.s.l. and produced the continuous map. The CAPS is an in-situ instrument, it was operated on the BN-2 and sampled the air at 300 m a.s.l. and performed vertical soundings above Magurele. The MPIC Mobile-DOAS mainly drove along the Bucharest ring road.

The different datasets of Fig. 7 appear consistent. First, they reveal large differences of NO_2 amounts on Sunday 30 August 2015 compared to Monday 31 August 2015. On Sunday afternoon, the NO_2 VCDs peak around 1.5 x 10^{16} molec cm^{-2}. On Monday, the NO_2 plume spread from the center to the northeast of the city. The observed NO_2 VCDs were smaller than the detection limit upwind and reach up to 3.5 x 10^{16} molec cm^{-2} inside the plume. The NO_2 vmr measured with the CAPS

https://doi.org/10.5194/amt-2019-496
Preprint. Discussion started: 6 February 2020


Atmospheric Measurement Techniques Discussions

was close to the detection limit on Sunday while it reached 5 ppb inside the plume on Monday 31 August 2015. Note that the systematic differences between AirMAP and the MPIC Mobile-DOAS at the eastern part of the ring road on 31 August 2015 were due to the time differences between both measurements. Meier (2018) compared the two instruments during the morning flights, which include more simultaneous observations. The comparison reveals a good agreement when averaging the forward and backward-looking Mobile-DOAS NO_2 VCDs, with a MPIC/AirMAP slope of 0.93 and a correlation coefficient of 0.94. Figure S6 in the Supplement presents this comparison.

Figure 8 presents collocated CAPS and AirMAP NO_2 measurements on 31 August 2015. The BN-2 carrying the CAPS flew from Magurele to the East of Bucharest, remaining outside the city ring at 300 m a.s.l. between 12:30 and 12:55 UTC, while AirMAP onboard the Cessna was mapping the city. We extracted the AirMAP NO_2 VCDs at the position of the CAPS observations. The figure confirms that the two instruments detected the plume at the same place. This suggests that along this portion of the flight, which was inside the plume but outside the city, the NO_2 vmr measured at 300 m a.s.l. may be used as a proxy for the NO_2 VCD. The BLH was about 1500m (Fig. 5) during these observations. Assuming a constant NO_2 vmr of 3.5 ppb leads to a NO_2 VCD of 1.4 x 10^{16} molec cm^{-2}. This estimation is close to the AirMAP NO_2 VCD observed in the plume (Fig. 8). Future campaigns should include vertical soundings inside the plume to further investigate its NO_2 vertical distribution.

3.1.4 Horizontal distribution of H_2CO

Figure 9 shows the H_2CO and NO_2 VCDs measurements from the Avantes spectrometer operated onboard the Cessna on 31 August 2015 (morning flight), together with the time-coincident MPIC Mobile-DOAS measurements. The H_2CO VCDs range between 1$\pm$0.25 x 10^{16} molec cm^{-2} and 7.5$\pm$2 x 10^{16} molec cm^{-2}, a maximum observed inside the city. We estimated the H_2CO reference column for the airborne data using the Mobile-DOAS measurements. Both NO_2 and H_2CO are in good agreement when comparing their distributions as seen from the airborne and ground-based instruments. However, if the highest H_2CO VCDs are found above the Bucharest city center, they are not coincident with the NO_2 maximum, as can be seen comparing the upper and lower panels of Fig. 9, for instance on the second Cessna flight line from the north.

The H_2CO hotspot observed above Bucharest is mainly anthropogenic. Indeed, biogenic emissions typically account for 1 to 2 x 10^{16} molec cm^{-2} (J.-F. Müller, personal communication), in agreement with the background VCDs measured by the Mobile-DOAS along the Bucharest ring. During the measurements, the wind was blowing from south and west. The difference between NO_2 and H_2CO spatial patterns may be explained by the different sources of NO_x compared to H_2CO or by the formation time of H_2CO through the oxidation of VOCs.

Anthropogenic hotspots of H_2CO have already been observed, e.g. above Houston (Texas), an urban area which includes significant emissions from transport and petrochemical industry (Parrish et al., 2012; Nowlan et al., 2018). Nowlan et al. also deployed an airborne DOAS nadir instrument, they reported H_2CO VCDs up to 5 x 10^{16} molec cm^{-2} in September 2013.

https://doi.org/10.5194/amt-2019-496
Preprint. Discussion started: 6 February 2020


Atmospheric Measurement Techniques Discussions

3.2 The Jiu Valley

3.2.1 Spatial distribution of NO_2

Figure 10 presents the horizontal distribution of the NO_2 VCDs in the Jiu Valley measured with the MPIC Mobile-DOAS on 23 August 2015. The figure shows elevated NO_2 VCDs close to the four power plants listed in Table 3, with up to 8x10^{16} molec cm^{-2} downwind of Turceni and Rovinari. In comparison, the area East of Craiova is very clean, with typical NO_2 VCDs under 1x10^{15} molec cm^{-2}.

The situation of Fig. 10 is characteristic of the conditions encountered in the Jiu Valley, with high NO_2 VCDs observed north and west of the plants due to the prevailing wind directions. During both campaigns, we observed maximum NO_2 VCDs reaching up to 1.3x10^{17} molec cm^{-2} close to the plants with Mobile-DOAS instruments.

Figure S3 in the Supplement shows the AirMAP and SWING NO_2 VCDs measured around the Turceni power plant on 28 August 2015. The two airborne instruments largely agree, detecting NO_2 VCDs up to 8x10^{16} molec cm^{-2} in the exhaust plume of the power plant. Figure S4 in the Supplement (upper panel) extracts the AirMAP and SWING NO_2 VCDs along the path of the simultaneous ground-based Mobile-DOAS measurements and compares the three datasets. This comparison confirms that there is a good agreement for the airborne instruments but indicates that comparing with Mobile-DOAS instruments is less straightforward. When observed with the Mobile-DOAS, the plume shows higher NO_2 VCDs and appears narrower than with the airborne instruments. This is partly related to air mass factor uncertainties, but probably also to 3-D effects as the plume is very thin and heterogeneous close the power plants, as discussed in Merlaud et al. (2018).

Figure 11 shows those AROMAT-1 NO_2 sonde measurements above Turceni which detected the plume. The NO_2 is not well-mixed in the boundary layer, with maxima aloft and lower vmrs close to the surface. This is understandable so close to the source, as high-temperature NO_x is emitted from the 280 m high stack. In these balloon-borne datasets, the observed maximum NO_2 vmr is about 60 ppb inside the plume, and the NO_2 vmr vanishes above 1200 m a.s.l.. These results suggest that airborne measurements with the ULM-DOAS, which can fly safely at 1500 m a.s.l., can provide reliable measurements of the integrated column amount inside the plume. Note that we measured NO_2 vmrs of up to 95 ppb on the ground at the soccer field (see Fig. S11 in the Supplement) when the wind was blowing from the power plant.

3.2.2 Horizontal distribution of SO_2

Figure 12 presents the SO_2 horizontal distributions measured around Turceni with AirMAP (left panel) and SWING (right panel) on 28 August 2015. The maps show the plume from the Turceni plant transported in the northwest direction, and other areas with elevated SO_2 VCDs in the east and south of Turceni. Meier (2018) presents in detail these AirMAP SO_2 observations and compares them with SWING results. It is found that the AirMAP-derived SO_2 columns inside the plume SO_2 reach 6x10^{17} molec cm^{-2} and that the AirMAP and SWING SO_2 VCDs agree within 10%. Moreover, for these airborne data, the SO_2 horizontal distribution broadly follows that of NO_2. The discrepancies can be explained by the different lifetimes of the two species.

https://doi.org/10.5194/amt-2019-496
Preprint. Discussion started: 6 February 2020


Atmospheric Measurement Techniques Discussions

We have measured higher SO_2 levels during AROMAT-2 than during AROMAT-1, both in terms of VCDs and vmrs, as shown in Fig. S10 of the supplement material. This corresponds to a shutdown of the desulfurization unit of the power plant, which local workers reported during the campaign. On 26 August 2015 in particular, the SO_2 vmr went up to 250 ppb, above the WMO guidelines of 191 ppb for the 10 minutes mean, while it never exceeded 50 ppb in 2014.

As for NO_2, it appears difficult to quantitatively relate the airborne and Mobile-DOAS SO_2 VCDs observations in the close vicinity of the power plant. As shown in Fig. S4 of the supplemental material (lower panel), the maximum SO_2 VCD measured from the ground on the road close to the factory amounts to 1.3 x 10^{18} molec cm^{-2} while from the aircraft, the SO_2 VCD reached 8 x 10^{17} molec cm^{-2}. Part of this difference can be explained by 3-D effects on the radiative transfer, as for NO_2. As discussed below, it seems easier to compare the SO_2 flux.

4 Discussion

This section addresses the lessons learned from our study for the validation of satellite observations of the three investigated tropospheric trace gases, namely NO_2, SO_2, and H_2CO. For each molecule, we discuss the added value of conducting such an airborne campaign as well as the choice of Romania as a campaign site. The last part of the section estimates the NO_x and SO_2 emissions from Bucharest and from the power plants of the Jiu Valley, using the different datasets of the campaigns.

4.1 Lessons learned for the validation of space-borne NO_2 VCDs

4.1.1 Number of possible pixels and dynamic range at the TROPOMI resolution

Regarding Bucharest, the mapped area of Fig. 7 virtually covers 43 TROPOMI near-nadir pixels. Averaging the high spatial resolution AirMAP NO_2 VCDs within these 43 hypothetical TROPOMI measurements reduces the dynamic range of the observed NO_2 field. The latter decreases from 3.5x10^{16} to 2.6x10^{16} molec cm^{-2} (37 σ where σ is the required precision on the tropospheric NO_2 VCD). Nevertheless, 33 of the 43 hypothetical TROPOMI pixels exhibits a NO_2 VCD above the required 2-σ random error for TROPOMI (1.4x10^{15} molec cm^{-2}).

Regarding the Jiu Valley, a similar exercise based on our measurments on 28 August 2012 (Fig.S3 in the Supplement) leads to 48 near-nadir TROPOMI pixels, out of which 35 would have a NO_2 VCD above the 2-σ TROPOMI error. The largest NO_2 tropospheric VCD seen by TROPOMI would be around 2x10^{16} molec cm^{-2} (29 σ for TROPOMI).

4.1.2 Characterization of the reference measurements

Table 4 summarizes the NO_2 observations during the AROMAT campaigns. For each instrument, the table indicates the measured range of NO_2 VCDs (or vmr), the ground sampling distance and a typical detection limit and bias. Regarding DOAS instruments, we estimated the detection limits on the NO_2 VCDs from typical 1-σ DOAS fit uncertainties divided by typical air mass factors (AMF). Table S1 in the Supplement presents these typical AMFs and detection limits. The 1-σ DOAS fit uncertainty is instrument specific and an output of the DOAS fitting algorithms. The AMF depends on the observation's geometry,

https://doi.org/10.5194/amt-2019-496
Preprint. Discussion started: 6 February 2020


Atmospheric Measurement Techniques Discussions

atmospheric and surface optical properties. Uncertainties on the AMF usually dominate the systematic part of the error for the DOAS measurements. Therefore, for these instruments, the bias given in Table 4 corresponds to the uncertainty in their associated AMF.

Combined with the ground sampling distance, the detection limit enables one to quantify the random uncertainty of a reference observation at the satellite horizontal resolution. Indeed, considering reference measurements averaged within a satellite pixel, the random error associated with the averaged reference measurements decreases with the square root of the number of measurements, following Poisson statistics. For instance, a continuous mapping performed with SWING at a spatial resolution of 300 x 300 m^2 inside a TROPOMI pixel of 3.5 x 5.5 km^2 would lead to 214 SWING pixels. Averaging the NO_2 VCDs of these SWING pixels would divide the SWING original uncertainty (1.2x10^{15} molec.cm^{-2}) by $\sqrt{214}$, leading to 8.2x10^{13} molec.cm^{-2}, about one tenth of the random error of TROPOMI (7x10^{14} molec.cm^{-2}) given in table 2.

However, the temporal variation of the NO_2 VCDs further adds uncertainty to the reference measurements when comparing them with satellite data. The validation areas typically extend over a few tens of kilometers. At this scale, satellite observations are a snapshot in time of the atmospheric state, while an airborne mapping typically takes one or two hours.

We investigated the temporal variation of the NO_2 VCDs comparing consecutive AirMAP overpasses above Bucharest from the morning flight of 31 August 2015. During this flight, the Cessna covered the same area three times in a row between 07:06 and 08:52 UTC. For each AirMAP overpass, we averaged the NO_2 VCDs at the horizontal resolution of TROPOMI (see previous section). The standard deviation of the differences between two averaged overpasses then indicates the random part of the NO_2 VCDs temporal variation during an aircraft overpass. This standard deviation is 3.7x10^{15} and 4.2x10^{15} molec cm^{-2}, respectively between the first and second, and second and third overpass. Hereafter, we used 4x10^{15} molec cm^{-2} as random error due to the temporal variation. Figure S10 in the Supplement illustrates these investigations on the temporal variation of the NO_2 VCDs at the TROPOMI resolution.

Clearly, the NO_2 VCD temporal variation depends on characteristics of a given validation experiments, such as the source locations and the wind conditions during the measurements. In the studied case however, this error source is larger for the reference measurements than the TROPOMI precision (7x10^{14} molec cm^{-2}). This is quite different from using static MAX-DOAS as reference. The latter are usually averaged within one hour around the satellite overpass. Compenolle et al. (paper in preparation) quantify the temporal error for MAX-DOAS NO_2 VCDs, typically ranging between 1 to 5x10^{14} molec cm^{-2}. Whether the reference is based on airborne or ground-based measurements, underestimating its temporal random error propagates in underestimating the slope between reference and satellite observations. For MAX-DOAS, this also happens when averaging the NO_2 VCDs within larger time windows around the satellite overpass (Wang et al., 2017).

4.1.3 Simulations of validation exercises in different scenarios

We simulated TROPOMI Cal/Val exercises with the spatially averaged AirMAP observations. We considered these averaged AirMAP NO_2 VCDs as the ground truth in simulated TROPOMI pixels, on which we added Gaussian noise to build synthetic satellite and reference NO_2 VCDs datasets. For the synthetic satellite observations, the noise standard deviation corresponded to the TROPOMI random error (the precision in Table 2). For the synthetic airborne observations, we added in quadrature

https://doi.org/10.5194/amt-2019-496
Preprint. Discussion started: 6 February 2020


Atmospheric Measurement Techniques Discussions

the aforementioned averaged airborne shot noise (e.g. 7x10^{13} molec cm^{-2} for SWING) and temporal error (4x10^{15} molec cm^{-2}, which we assumed to be also realistic around Turceni). We then applied orthogonal distance regressions to a series of such simulations to estimate the uncertainty on the regression slope. This led to slope uncertainties of about 6% and 10% in Bucharest and Turceni, respectively.

In a real-world validation experiment, this regression slope would quantify the combined biases of the two NO_2 VCDs datasets (satellite and reference). These biases mainly originate from errors in the AMFs, resulting in particular from uncertainties on the NO_2 and aerosol profiles, and on the surface albedo. To some extent, these quantities can be measured from an aircraft with the type of instrumentation deployed in the AROMAT activity. The ground albedo can be retrieved with the DOAS instruments by normalizing uncalibrated airborne radiances to a reference area with known albedo (Meier et al., 2017) or by using a radiometrically calibrated DOAS sensor (Tack et al., 2019). The NO_2 and aerosol profiles can be measured with in-situ instruments such as a CAPS NO_2 monitor and a nephelometer. For legal reasons, vertical soundings are difficult above cities. One can measure the NO_2 and aerosol profile further down in the exhaust plume, once the latter is above rural areas. The conditions inside the city can be different and this motivates the deployment of ground-based instruments, e.g. sunphotometers and MAX-DOAS, inside the city.

Regarding uncertainties on the references AMFs, the added value of knowing the aerosol and NO_2 profile appears when comparing the AMF error budget for airborne measurements above Bucharest (26%, Meier et al. (2017)) and above the Turceni power plant (10%, Merlaud et al. (2018)). In the latter case, there was accurate information on the local NO_2 and aerosol profiles thanks to the lidar and the balloon-borne NO_2 sonde, respectively. We used these two AMF uncertainties to estimate a total possible bias between reference and satellite observations.

Table 7 summarizes this section and presents total error budgets for different scenarios of validation exercises using reference airborne mapping to validate spaceborne tropospheric NO_2 VCDs. We estimated the random and systematic uncertainties between satellite and reference measurements with SWING and AirMAP, including (or not) profile information on the aerosols and NO_2 vmr, and for measurements over Bucharest or Turceni. Note that we considered 25% for the satellite accuracy. The temporal error of the airborne measurements clearly dominates the total random error, making the differences in detection limit between AirMAP and SWING irrelevant for this application. Adding the profile information on the other hand reduces the total multiplicative bias from 37% to 28% or 29% in Bucharest and Turceni. This quantifies the capabilities of such airborne measurements for the validation of the imaging capabilities of TROPOMI regarding the NO_2 VCDs above Bucharest and the Jiu Valley.

4.2 Lessons learned for the validation of space-borne H_2CO VCDs

Table 5 is similar to Table 4 but for H_2CO, which we only measured in significant amounts in and around Bucharest.

The background level of the H_2CO VCD around the city is around 1x10^{16} molec cm^{-2} and the anthropogenic increase in the city center is up to 7x10^{16} molec cm^{-2} (Fig. 9). The background falls within the TROPOMI H_2CO spread (1.2x10^{16} molec cm^{-2}), and Fig. 9 indicates that the extent of the urban hotspot only corresponds to a few TROPOMI pixels, with a maximum at 6 σ. This limits the relevance of individual mapping flights for the validation of H_2CO. The information on the

https://doi.org/10.5194/amt-2019-496
Preprint. Discussion started: 6 February 2020


Atmospheric Measurement Techniques Discussions

H_2CO horizontal variability is nevertheless useful, as it justifies the installation of a second MAX-DOAS in the city center, in addition to background measurements outside the city. Indeed, long-term ground-based measurements at two sites would be useful to investigate seasonal variations of H_2CO. Averaging the H_2CO over a season would reduce the random errors of the satellite measurements and it could reveal the horizontal variability of H_2CO from space. The H_2CO hotspot around Bucharest seems to be visible in the TROPOMI data of summer 2018 (I. De Smedt, personnal communication).

Getting information on the profile of H_2CO during an airborne campaign may also help to understand the differences between ground-based and space-borne observations. This could be done by adding to the BN-2 instrumental set-up an in-situ H_2CO sensor such as the In Situ Airborne Formaldehyde instrument (ISAF, Cazorla et al. (2015)) or the COmpact Formaldehyde FluorescencE Experiment (COFFEE, St. Clair et al. (2017)).

4.3 Lessons learned for the validation of space-borne SO_2 VCDs

Table 6 is similar to Table 4 but for SO_2, which we only measured in significant amounts in the Jiu Valley. The higher bias of the airborne measurements for SO_2 compared to NO_2 is due to the albedo. The latter is lower in the UV where we retrieve SO_2, which leads, for the same albedo error, to a larger AMF uncertainty (e.g. Merlaud et al., 2018, Fig.10).

Averaging the SO_2 VCDs from the airborne mapping of Fig. 12 at the TROPOMI resolution leads to 30 near nadir TROPOMI pixels above a 2-σ error of 5.4x10^{16} molec cm^{-2}. The maximum SO_2 tropospheric VCD seen by TROPOMI would be 2.4x10^{17} molec cm^{-2} (7 σ). This tends to indicate that airborne mappings of SO_2 VCDs above large power plants could help to validate the horizontal variability of the SO_2 VCDs measured from space, to a limited extent in the AROMAT conditions due to the small dynamic range (7 σ).

However, it would be difficult to quantify the bias of the satellite SO_2 VCD with AROMAT-type of airborne measurements. Adding in quadrature the biases of the SO_2 VCDs for airborne measurements (40%, Table 6) and for TROPOMI (30%, Table 2) already leads to a combined uncertainty of 50%, without considering any temporal variation or regression error. This best-case scenario is already at the upper limit of the TROPOMI requirements for tropospheric SO_2 VCDs (Table 2).

As for H_2CO, the validation of the satellite-based SO_2 measurements should thus rely on ground-based measurements, enabling to improve the signal-to-noise ratio of the satellite and reference measurements by averaging their time series. An additional difficulty for validating SO_2 VCDs emitted by a power plant arise from the spatial heterogeneity of the SO_2 field around the point source, which renders ground-based VCDs measurements complicated. On the other hand, Fioletov et al. (2017) presented a method to derive the SO_2 emissions from OMI data and validated it against reported emissions. The SO_2 fluxes can be measured locally in several ways and we tested some of them during AROMAT-2 (see Sect. 4.4.2 below). To validate satellite-derived SO_2 products in Europe, it thus seems possible to compare satellite and ground-based reference SO_2 fluxes. Theys et al. (2019) already validated TROPOMI-derived volcanic SO_2 fluxes against ground-based measurements. In this context, a SO_2 camera pointing to the plant stack would be a valuable tool since it could be permanently installed and automated. One advantage of such a camera compared to the other tested remote-sensing instruments, beside its low operating cost, is that it derives the extraction speed from the measurements, avoiding dependence on low-resolution wind information.

https://doi.org/10.5194/amt-2019-496
Preprint. Discussion started: 6 February 2020


Atmospheric Measurement Techniques Discussions

Note that since the desulfurization unit of the Turceni power plant was not fully operational during AROMAT-2, the SO_2 VCDs detected above Turceni on 28 August 2015 are expectedly higher than for standard conditions, all the more so as the SO_2 VCDs in the area seem to have further decreased (D. Constantin, personnal communication). The first reported TROPOMI SO_2 measurements above the area pinpoint other power plants in Serbia, Bosnia–Herzegovina, and Bulgaria (Fioletov et al., 2020). For validation studies, it would be worth to install automatic SO_2 cameras around these plants, until they are equiped with FGD units.

4.4 Emissions of NO_x and SO_2 emissions from Bucharest and the Jiu Valley

4.4.1 NO_x flux from Bucharest

We estimated NO_x fluxes from the Bucharest urban area using the NO_2 VCDs measured with the Mobile-DOAS systems along the external ring and the wind data on 8 September 2014 and 31 August 2015. We derived the wind direction from the maxima of the NO_2 VCDs in the DOAS observations. For the wind speed, we took 1.1 m s^{-1} on 8 September 2014, the value Meier (2018) used for the AirMAP-derived flux, which originates from meteorological measurements at Baneasa airport. On 31 August 2015, we used the ERA5 wind data (C3S, 2017) at the time when the Mobile-DOAS crossed the NO_2 plume (15:00 UTC). The ERA5 database indicates a constant windspeed between 1000 and 900 hPA of 1.2 m s^{-1}. Finally and similarly to Meier (2018), we took a ratio of 1.32 for the NO_x to NO_2 ratio and estimated the chemical loss of NO_x with a lifetime of 3.8h and an effective source location in the center of Bucharest.

Table 8 presents the AirMAP and Mobile-DOAS derived NO_x fluxes from Bucharest, ranging between 12.5 and 17.5 mol.s^{-1}. On 8 September 2014, the Mobile and airborne observations were coincident. Their estimated NO_x fluxes agree within 20%. This gives confidence in the flux estimation yet one should keep in mind that the same wind data was used for both estimations. Meier (2018) estimated the uncertainties on the AirMAP-derived NO_x flux to be around 63%, while the uncertainty of Mobile-DOAS derived NO_x flux typically range between 30% and 50% (Shaiganfar et al., 2017).

We compared our measured NO_x fluxes with the European Monitoring and Evaluation Programme inventory (EMEP, https://www.ceip.at/). In practice, we summed the EMEP gridded yearly NO_x emissions between 44.2°and 44.6°N and between 25.9 °E and 26.3 °E and we assumed the emissions are constant during one year. This led to NO_x emissions of 6.14 and 6.33 mol s^{-1} for 2014 and 2015. Studying the reported emissions from several European cities including Bucharest, Trombetti et al. (2018) mentions that the EMEP emissions are well below other inventories for all the pollutants. We thus also compared our flux with the Emissions Database for Global Atmospheric Research (EDGAR v4.3.2, Crippa et al. (2018)), which is only available until 2012. The same method led to a NO_x flux of 18.4 mol s^{-1}, to compared with the 2012 EMEP NO_x emissions of 7.1 mol s^{-1}. Based on summer measurements, the AROMAT-derived NO_x emissions do not include residential heating. The latter ranges between 10 and 40% of the total NO_x according to Trombetti et al. (2018). This tends to confirm that the EMEP inventory underestimates the NO_x emissions for Bucharest.

https://doi.org/10.5194/amt-2019-496
Preprint. Discussion started: 6 February 2020

Atmospheric Measurement Techniques Discussions

4.4.2 NO_x and SO_2 fluxes from the power plants in the Jiu Valley

We estimated the NO_x and SO_2 flux from the power plants using several instruments: a Mobile-DOAS, the ULM-DOAS, and the SO_2 camera. For the DOAS instruments, we inferred the wind direction from the plume position and we retrieved the wind speed from the ERA5 database. Considering the observed vertical extent of the plume downwind of Turceni (Fig. 11), we took the wind speed at 950 hPa (ca. 500 m a.s.l.).

Figure 14 presents the ULM-DOAS-estimated fluxes of NO_x and SO_2 from the power plants in Turceni, Rovinari, and Craiova for the flight on 26 August 2015. The figure also shows the reported emissions from the European Environment Agency (EEA) large combustion plants database (EEA, 2018), assuming constant emissions throughout the year. Turceni appears to be the largest SO_2 source (78 mol s^{-1}), while Rovinari is the largest NO_x source (8 mol s^{-1}).

It is difficult to interpret the discrepancies between those measured fluxes and the yearly reported emissions since we observed large variations in the instantaneous emissions with the SO_2 camera (see below and Fig. 13). However, the ratio of the two fluxes appears interesting since we can assume its relative stability. This ratio for a given power plant depends on whether or not a desulfurization unit is operational at the plant. On Fig. 14, Turceni appears to have both the largest measured ratio and the largest discrepancy between the measured and reported ratios. This is consistent with a temporary shutdown of the desulfurization unit of the Turceni power plant, as was reported by the plant workers during the campaign. The ULM-DOAS measurements on 25 August 2015 (shown in Fig.S14 the Supplement), which also sampled the Isalnita plume, indicates that the desulfurization unit may not have been operational there either. The ULM-DOAS measurements on 25 August 2015, which covered the four power plants, enable to estimate total NO_x and SO_2 fluxes to be about 22 and 147 mol s^{-1}, respectively.

Table 9 focuses on the Turceni power plant and lists all estimates of the NO_x and SO_2 emissions from this source. Meier (2018) estimated the NO_x flux from the Turceni power plant using the AirMAP measurements of 2014 and 2015. This leads to similar values for the two flights on 11 September 2014 and 28 August 2015, of about 8 mol.s^{-1}. On this second day, the UGAL Mobile-DOAS crossed the plume along the road in front of the power plant. These ground-based measurements lead to a NO_2 flux of 2.2 mol.s^{-1}, much lower than the aforementioned AirMAP-derived value. However, Meier (2018) calculated the latter based on AirMAP measurements at 3.5 km from the source. At shorter distances, the AirMAP estimated NO_2 flux is smaller and close to the Mobile-DOAS observations. This is probably related to the fact that the NO/NO_2 ratio has not yet reached its steady state value above the road where we performed the Mobile-DOAS observations, which is only around 1 km from the stack. The agreement is better for SO_2 (25 and 32 mol.s^{-1}). On 25 August 2015, we had a coincidence of ULM-DOAS and Mobile-DOAS observations and we observed a similar range of values. This gives us confidence in our estimate of the NO_x flux from the aircraft but confirms that the nearby road is too close to the plant to estimate a meaningful NO_x flux from Mobile-DOAS NO_2 observations. Note that the conversion of NO into NO_2 is also visible right above the Turceni stack in the NO_2 imager data of 24 August 2015, as appears in Fig.6 of Dekemper et al. (2016).

Figure 13 presents a time series of the SO_2 emissions from the Turceni power plant between 9:00 and 10:50 UTC on 28 August 2015. We derived SO_2 fluxes at different altitudes above the stack using a UV SO_2 camera which is an updated version of the Envicam2 system, used during the SO_2 camera intercomparison described by Kern et al. (2015). We converted the

https://doi.org/10.5194/amt-2019-496
Preprint. Discussion started: 6 February 2020


Atmospheric Measurement Techniques Discussions

measured optical densities to SO_2 column densities using simultaneous measurements with an integrated USB spectrometer (Lübcke et al., 2013). We estimated the stack exit velocity from the SO_2 images, recorded with a time resolution of about 15 seconds, by tracking the spatial features of the plume. Dekemper et al. (2016) used a similar approach to derive the NO_2 flux from NO_2 camera imagery.

The SO_2 fluxes retrieved for transverses at 400 to 700 m vertical distances above the stack agree on average with each other within 20%. Emissions estimated 100 m above the stack are underestimated due to saturation (SO_2 column densities above 2 x 10^{18} molec.cm^{-2}) and high aerosol concentration close to the exhaust.

The SO_2 emissions show large fluctuations. During the time of our observations they increased from 1 kg.s^{-1} (15.6 mol.s^{-1}) to around 4 $\pm$ 1 kg^{-1} (62.4 mol.s^{-1}). The images (Fig.S13 in the supplement) also show a second and weaker source that emits SO_2. This is probably the desulfurization unit, which was reported to be turned on again on this day, after the temporary shutdown. Indeed, as appears in Table 9, the SO_2/NO_2 ratio measured from AirMAP is lower than the ones measured from the ULM-DOAS during the previous days, and the same holds true for the Mobile-DOAS measurements.

5 Conclusions

The two AROMAT campaigns took place in Romania in September 2014 and August 2015. These campaigns combined airborne and ground-based atmospheric measurements and focused on air quality-related species (NO_2, SO_2, H_2CO, and aerosols). The AROMAT activity targeted the urban area of Bucharest and the power plants of the Jiu Valley. The campaigns aimed at testing new instruments, measuring the concentrations and emissions of key pollutants in the two areas, and investigating the concept of such campaigns for the validation of air quality satellite-derived products.

We have shown that the airborne mapping of tropospheric NO_2 VCDs above Bucharest is potentially valuable for the validation of current and future nadir-looking satellite instruments. These measurements agree with ground-based measurements and cover a significant part of the dynamic range of the NO_2 tropospheric VCDs at an appropriate signal to noise ratio, enabling to constrain the accuracy of the satellite NO_2 VCDs within 37 or 28%, with and without information on the aerosol and NO_2 profile, respectively. This points out the importance of the profile information to approach the TROPOMI optimal target accuracy for tropospheric NO_2 VCDs (25%).

A unique advantage of airborne mapping is its ability to validate the imaging capabilities of nadir-looking satellites. This feature becomes more important as the satellite horizontal resolutions reaches the suburban scale. Judd et al. (2019) pointed out the difficulty for static ground-based measurements to represent the NO_2 VCDs measured from space in polluted areas, due to the horizontal representativeness error. This error cancels out by mapping the full extent of satellite pixels. The caveat is the temporal error, which can be larger than with static ground-based measurements. We have estimated the temporal error to be about 4 x 10^{15} molec cm^{-2} in our observations above Bucharest, but it varies with local conditions for a given experiment. This indicates the usefulness of simultaneous ground-based measurements, which may also be useful to estimate the reference NO_2 VCDs in the airborne observations.

https://doi.org/10.5194/amt-2019-496
Preprint. Discussion started: 6 February 2020


Atmospheric Measurement Techniques Discussions

We also detected a clear signal of H_2CO in and around Bucharest, with an anthropogenic hotspot in the city center. Due to the lower signal to noise ratio of the spaceborne H_2CO observations, this structure is not visible in daily satellite measurements. We thus propose considering long-term ground-based MAX-DOAS measurements in the city for the validation of H_2CO.

In the Jiu Valley, NO_2 is clearly visible from both satellite and aircraft, and the VCDs are comparable in magnitude with the signal detected above Bucharest. However, it appears more complicated to quantitatively compare the NO_2 VCDs datasets in the thick exhaust plumes of the power plants. These plants also emit SO_2 but, as for H_2CO, the low signal to noise ratio of satellite measurements reduces the validation relevance of individual airborne measurements. As the SO_2 emissions have been drastically reduced with the installation of flue-gas desulfurization units in the Jiu Valley, we propose targeting SO_2 emissions from other coal-fired power plants having higher emissions, e.g. in Serbia.

Considering the optimal validation study mentioned in the introduction, the validation relevance of an international airborne campaign is usually limited by its timespan of typically a couple of weeks, imposed in practice by cost considerations. To overcome this limitation, one might consider routine airborne mapping of NO_2 VCDs by local aircraft operators, close to a well-equipped ground-based observatory. Such a set-up would reduce the fixed costs of the observations, which could be allocated to flight hours in different seasons. This would combine the advantages of long-term ground-based and airborne measurements. In the longer term, high altitude pseudo-satellites (HAPS) could help to achieve such routine measurements above selected supersites, which would be particularly valuable to validate the observations from geostationary satellites.

Competing interests. The authors declare that they have no conflict of interest.

Author contributions. AM, LB, D-EC, MDH, ACM, LG, DN, and MVR planned and organised the campaign. All coauthors contributed to the campaign either as participants or during campaign preparation and/or follow up data analysis, including the writing of this manuscript, which was coordinated by AM and MVR with feedback and contributions from all the coauthors.

Acknowledgements. The AROMAT activity was supported by ESA (contract $4000113511/15/NL/FF/gp$) and by the Belgian Science Policy (contract $BR/121/PI/UAV Reunion$). Regarding the AirMAP instrument, financial support through the University of Bremen Institutional Strategy Measure M8 in the framework of the DFG Excellence Initiative is gratefully acknowledged. Part of the work performed for this study was funded by the Romanian Ministry of Research and Innovation through Program I - Development of the national research-development system, Subprogram 1.2 - Institutional Performance - Projects of Excellence Financing in RDI, Contract No.19PFE / 17.10.2018 and by Romanian National Core Program Contract No.18N/2019. Katharina Riffel supported the MPIC mobile DOAS measurements. We thank Klaus Pfeilsticker, Isabelle De Smedt, Nicolas Theys, Ermioni Dimitropoulou, and Lori Neary for useful discussions. We also thank the people of Turceni and the Air Traffic Control of Romania for their support and cooperation.

https://doi.org/10.5194/amt-2019-496
Preprint. Discussion started: 6 February 2020

Atmospheric Measurement Techniques Discussions

References

Alpopi, C. and Colesca, S. E.: Urban air quality. A comparative study of major European capitals, Theoretical and Empirical Researches in Urban Management, 5, 92–107, 2010.

Bauwens, M., Stavrakou, T., Müller, J.-F., De Smedt, I., Van Roozendael, M., van der Werf, G. R., Wiedinmyer, C., Kaiser, J. W., Sindelarova, K., and Guenther, A.: Nine years of global hydrocarbon emissions based on source inversion of OMI formaldehyde observations, Atmos. Chem. Phys., 16, https://doi.org/10.5194/acp-16-10133-2016, 2016.

Belegante, L., Nicolae, D., Nemuc, A., Talianu, C., and Derognat, C.: Retrieval of the boundary layer height from active and passive remote sensors. Comparison with a NWP model, Acta Geophysica, 62, 276–289, https://doi.org/10.2478/s11600-013-0167-4, 2014.

Boersma, K. F., Eskes, H. J., Dirksen, R. J., van der A, R. J., Veefkind, J. P., Stammes, P., Huijnen, V., Kleipool, Q. L., Sneep, M., Claas, J., Leitão, J., Richter, A., Zhou, Y., and Brunner, D.: An improved tropospheric NO_2 column retrieval algorithm for the Ozone Monitoring Instrument, Atmos. Meas. Tech., 4, 1905–1928, https://doi.org/10.5194/amt-4-1905-2011, 2011.

Boersma, K. F., Vinken, G. C. M., and Tournadre, J.: Ships going slow in reducing their NOx emissions: changes in 2005–2012 ship exhaust inferred from satellite measurements over Europe, Environmental Research Letters, 10, 074 007, https://doi.org/10.1088/1748-9326/10/7/074007, 2015.

Boersma, K. F., Eskes, H. J., Richter, A., De Smedt, I., Lorente, A., Beirle, S., van Geffen, J. H. G. M., Zara, M., Peters, E., Van Roozendael, M., Wagner, T., Maasakkers, J. D., van der A, R. J., Nightingale, J., De Rudder, A., Irie, H., Pinardi, G., Lambert, J.-C., and Compernolle, S. C.: Improving algorithms and uncertainty estimates for satellite NO_2 retrievals: results from the quality assurance for the essential climate variables (QA4ECV) project, Atmospheric Measurement Techniques, 11, 6651–6678, https://doi.org/10.5194/amt-11-6651-2018, https://www.atmos-meas-tech.net/11/6651/2018/, 2018.

Bösch, T., Meier, A., Schönhardt, A., Peters, E., Richter, A., Ruhtz, T., and Burrows, J.: Airborne measurements of different trace gases during the AROMAT-2 campaign with an Avantes spectrometer, in: EGU General Assembly, Vienna, Austria, 17–22 April 2016, pp. EGU2016–7394, 2016.

Brenot, H., Theys, N., Clarisse, L., Geffen, J. V., Gent, J. V., Roozendael, M. V., and Hurtmans, D.: Support to Aviation Control Service (SACS): an online service for near-real-time satellite monitoring of volcanic plumes, pp. 1099–1123, https://doi.org/10.5194/nhess-14-1099-2014, 2014.

Brinksma, E. J., Pinardi, G., Volten, H., Braak, R., Richter, A., Schönhardt, A., van Roozendael, M., Fayt, C., Hermans, C., Dirksen, R. J., Vlemmix, T., Berkhout, A. J. C., Swart, D. P. J., Oetjen, H., Wittrock, F., Wagner, T., Ibrahim, O. W., de Leeuw, G., Moerman, M., Curier, R. L., Celarier, E. A., Cede, A., Knap, W. H., Veefkind, J. P., Eskes, H. J., Allaart, M., Rothe, R., Piters, A. J. M., and Levelt, P. F.: The 2005 and 2006 DANDELIONS NO2 and aerosol intercomparison campaigns, J. Geophys. Res., 113, https://doi.org/10.1029/2007JD008808, 2008.

Burrows, J. P., Weber, M., Buchwitz, M., Rozanov, V., Ladstätter-Weißenmayer, A., Richter, A., DeBeek, R., Hoogen, R., Bramstedt, K., Eichmann, K.-U., Eisinger, M., Perner, D., Burrows, J. P., Weber, M., Buchwitz, M., Rozanov, V., Ladstätter-Weißenmayer, A., Richter, A., DeBeek, R., Hoogen, R., Bramstedt, K., Eichmann, K.-U., Eisinger, M., and Perner, D.: The Global Ozone Monitoring Experiment (GOME): Mission Concept and First Scientific Results, J. Atmospheric Sci., 56, https://doi.org/10.1175/1520-0469(1999)056<0151:TGOMEG>2.0.CO;2, 1999.

C3S: ERA5: Fifth generation of ECMWF atmospheric reanalyses of the global climate. Copernicus Climate Change Service Climate Data Store (CDS), accessed 24 September 2019, 2017.

https://doi.org/10.5194/amt-2019-496
Preprint. Discussion started: 6 February 2020

Cazorla, M., Wolfe, G. M., Bailey, S. A., Swanson, A. K., Arkinson, H. L., and Hanisco, T. F.: A new airborne laser-induced fluorescence instrument for in situ detection of formaldehyde throughout the troposphere and lower stratosphere, Atmos. Meas. Tech., 8, 541–552, https://doi.org/10.5194/amt-8-541-2015, 2015.

Chance, K., Liu, X., Suleiman, R. M., Flittner, D. E., Al-Saadi, J., and Janz, S. J.: Tropospheric emissions: monitoring of pollution (TEMPO), p. 88660D, International Society for Optics and Photonics, https://doi.org/10.1117/12.2024479, 2013.

Constantin, D., Merlaud, A., Van Roozendael, M., Voiculescu, M., Fayt, C., Hendrick, F., Pinardi, G., and Georgescu, L.: Measurements of Tropospheric NO2 in Romania Using a Zenith-Sky Mobile DOAS System and Comparisons with Satellite Observations, Sensors, 13, 3922–3940, https://doi.org/10.3390/s130303922, 2013.

Constantin, D., Voiculescu, M., Dragomir, C., Georgescu, L., Merlaud, A., and Van Roozendael, M.: Measurements of NO2 using a Mobile DOAS system in Gorj county, Romania, The 18th International Conference TEHNOMUS, 2015.

Constantin, D.-E., Merlaud, A., Voiculescu, M., Dragomir, C., Georgescu, L., Hendrick, F., Pinardi, G., and Van Roozendael, M.: Mobile DOAS Observations of Tropospheric NO2 Using an UltraLight Trike and Flux Calculation, Atmosphere, 8, 78, https://doi.org/10.3390/atmos8040078, 2017.

Crippa, M., Guizzardi, D., Muntean, M., Schaaf, E., Dentener, F., van Aardenne, J. A., Monni, S., Doering, U., Olivier, J. G. J., Pagliari, V., and Janssens-Maenhout, G.: Gridded emissions of air pollutants for the period 1970–2012 within EDGAR v4.3.2, Earth Syst. Sci. Data, 10, 1987–2013, https://doi.org/10.5194/essd-10-1987-2018, 2018.

De Smedt, I., Müller, J.-F., Stavrakou, T., van der A, R., Eskes, H., and Van Roozendael, M.: Twelve years of global observations of formaldehyde in the troposphere using GOME and SCIAMACHY sensors, Atmos. Chem. Phys., 8, 4947–4963, https://doi.org/10.5194/acp-8-4947-2008, 2008.

Dekemper, E., Vanhamel, J., Van Opstal, B., and Fussen, D.: The AOTF-based NO2 camera, Atmos. Meas. Tech., 9, 6025–6034, https://doi.org/10.5194/amt-9-6025-2016, 2016.

Donner, S., Lampel, J., Shaiganfar, R., Gu, M., and T, W.: Construction and characterisation of a new compact MAX-DOAS instrument—Correction of detector non-linearity, in: 7th international DOAS workshop, Brussels, Belgium, 2015.

Drosoglou, T., Koukouli, M. E., Kouremeti, N., Bais, A. F., Zyrichidou, I., Balis, D., van der A, R. J., Xu, J., and Li, A.: MAX-DOAS NO_2 observations over Guangzhou, China; ground-based and satellite comparisons, Atmos. Meas. Tech., 11, 2239–2255, https://doi.org/10.5194/amt-11-2239-2018, 2018.

EEA: Reported information on large combustion plants, Tech. Rep. 4.2, European Environment Agency, Copenhagen, Denmark, 2018.

EEA: Air quality in Europe -2019 report, Tech. Rep. 10.2019, European Environment Agency, Copenhagen, Denmark, 2019.

Eisinger, M. and Burrows, J. P.: Tropospheric sulfur dioxide observed by the ERS-2 GOME instrument, Geophys. Res. Lett., 25, 4177–4180, https://doi.org/10.1029/1998GL900128, 1998.

ESA: Requirements for the Geophysical Validation of Sentinel-5 Precursor Products, Tech. Rep. S5P-RS-ESA-SY-164, European Space Agency, Noordwijk, The Netherlands, 2014.

Fioletov, V., McLinden, C. A., Kharol, S. K., Krotkov, N. A., Li, C., Joiner, J., Moran, M. D., Vet, R., Visschedijk, A. J. H., and Denier van der Gon, H. A. C.: Multi-source SO_2 emission retrievals and consistency of satellite and surface measurements with reported emissions, Atmos. Chem. Phys., 17, 12 597–12 616, https://doi.org/10.5194/acp-17-12597-2017, 2017.

Fioletov, V., McLinden, C. A., Griffin, D., Theys, N., Loyola, D. G., Hedelt, P., Krotkov, N. A., and Li, C.: Anthropogenic and volcanic point source SO_2 emissions derived from TROPOMI onboard Sentinel 5 Precursor: first results, Atmos. Chem. Phys. Discuss., 2020, 1–30, https://doi.org/10.5194/acp-2019-1095, 2020.

https://doi.org/10.5194/amt-2019-496
Preprint. Discussion started: 6 February 2020

Griffin, D., Zhao, X., McLinden, C. A., Boersma, F., Bourassa, A., Dammers, E., Degenstein, D., Eskes, H., Fehr, L., Fioletov, V., Hayden, K., Kharol, S. K., Li, S.-M., Makar, P., Martin, R. V., Mihele, C., Mittermeier, R. L., Krotkov, N., Sneep, M., Lamsal, L. N., Linden, M. t., Geffen, J. v., Veefkind, P., and Wolde, M.: High-Resolution Mapping of Nitrogen Dioxide With TROPOMI: First Results and Validation Over the Canadian Oil Sands, Geophys. Res. Lett., 46, 1049–1060, https://doi.org/10.1029/2018GL081095, 2019.

Grigoraş, G., Ştefan, S., Rada, C., and Grigoraş, C.: Assessing of surface-ozone concentration in Bucharest, Romania, using OML and satellite data, Atmos. Pollut. Res., 7, 567–576, https://doi.org/10.1016/j.apr.2016.02.001, 2016.

Heland, J., Schlager, H., Richter, A., and Burrows, J. P.: First comparison of tropospheric NO2 column densities retrieved from GOME measurements and in situ aircraft profile measurements, Geophys. Res. Lett., 29, https://doi.org/200210.1029/2002GL015528, 2002.

Heue, K. P., Richter, A., Bruns, M., Burrows, J. P., v. Friedeburg, C., Platt, U., Pundt, I., Wang, P., and Wagner, T.: Validation of SCIAMACHY tropospheric NO2 columns with AMAXDOAS measurements, Atmos. Chem. Phys., 5, 1039–1051, https://doi.org/10.5194/acp-5-1039-2005, 2005.

Hönninger, G., von Friedeburg, C., and Platt, U.: Multi axis differential optical absorption spectroscopy (MAX-DOAS), Atmos. Chem. Phys., 4, 231–254, https://doi.org/10.5194/acp-4-231-2004, 2004.

Ingmann, P., Veihelmann, B., Langen, J., Lamarre, D., Stark, H., and Courrèges-Lacoste, G. B.: Requirements for the GMES Atmosphere Service and ESA's implementation concept: Sentinels-4/-5 and -5p, Remote Sensing of Environment, 120, 58–69, https://doi.org/10.1016/j.rse.2012.01.023, 2012.

Irie, H., Kanaya, Y., Akimoto, H., Tanimoto, H., Wang, Z., Gleason, J. F., and Bucsela, E. J.: Validation of OMI tropospheric NO2 column data using MAX-DOAS measurements deep inside the North China Plain in June 2006: Mount Tai Experiment 2006, Atmos. Chem. Phys., 8, https://doi.org/10.5194/acp-8-6577-2008, 2008.

Judd, L. M., Al-Saadi, J. A., Valin, L. C., Pierce, R. B., Yang, K., Janz, S. J., Kowalewski, M. G., Szykman, J. J., Tiefengraber, M., and Mueller, M.: The Dawn of Geostationary Air Quality Monitoring: Case Studies From Seoul and Los Angeles, Frontiers in Environmental Science, 6, 85, https://doi.org/10.3389/fenvs.2018.00085, 2018.

Judd, L. M., Al-Saadi, J. A., Janz, S. J., Kowalewski, M. G., Pierce, R. B., Szykman, J. J., Valin, L. C., Swap, R., Cede, A., Mueller, M., Tiefengraber, M., Abuhassan, N., and Williams, D.: Evaluating the impact of spatial resolution on tropospheric NO_2 column comparisons within urban areas using high-resolution airborne data, Atmos. Meas. Tech. Discuss., 2019, 1–25, https://doi.org/10.5194/amt-2019-161, 2019.

Kanaya, Y., Irie, H., Takashima, H., Iwabuchi, H., Akimoto, H., Sudo, K., Gu, M., Chong, J., Kim, Y. J., Lee, H., Li, A., Si, F., Xu, J., Xie, P.-H., Liu, W.-Q., Dzhola, A., Postylyakov, O., Ivanov, V., Grechko, E., Terpugova, S., and Panchenko, M.: Long-term MAX-DOAS network observations of NO2 in Russia and Asia (MADRAS) during the period 2007-2012: instrumentation, elucidation of climatology, and comparisons with OMI satellite observations and global model simulations, Atmos. Chem. Phys., 14, https://doi.org/10.5194/acp-14-7909-2014, 2014.

Kebabian, P. L., Herndon, S. C., and Freedman, A.: Detection of nitrogen dioxide by cavity attenuated phase shift spectroscopy, Anal. Chem., 77, 724–728, https://doi.org/10.1021/ac048715y, 2005.

Kern, C., Lübcke, P., Bobrowski, N., Campion, R., Mori, T., Smekens, J.-F., Stebel, K., Tamburello, G., Burton, M., Platt, U., and Prata, F.: Intercomparison of SO2 camera systems for imaging volcanic gas plumes, J. Volcanol. Geotherm. Res., 300, 22 – 36, https://doi.org/https://doi.org/10.1016/j.jvolgeores.2014.08.026, 2015.

Kim, J.: GEMS(Geostationary Environment Monitoring Spectrometer) onboard the GeoKOMPSAT to Monitor Air Quality in high Temporal and Spatial Resolution over Asia-Pacific Region, in: EGU2012-4051, EGU General Assembly, 2012.

https://doi.org/10.5194/amt-2019-496
Preprint. Discussion started: 6 February 2020

Atmospheric Measurement Techniques Discussions

Kim, S.-W., Heckel, A., Frost, G. J., Richter, A., Gleason, J., Burrows, J. P., McKeen, S., Hsie, E.-Y., Granier, C., and Trainer, M.: NO2 columns in the western United States observed from space and simulated by a regional chemistry model and their implications for NOx emissions, Journal of Geophysical Research: Atmospheres, 114, https://doi.org/10.1029/2008JD011343, 2009.

Kowalewski, M. G. and Janz, S. J.: Remote sensing capabilities of the GEO-CAPE airborne simulator, 9218, 92 181I, https://doi.org/10.1117/12.2062058, 2014.

Krotkov, N. A., McLinden, C. A., Li, C., Lamsal, L. N., Celarier, E. A., Marchenko, S. V., Swartz, W. H., Bucsela, E. J., Joiner, J., Duncan, B. N., Boersma, K. F., Veefkind, J. P., Levelt, P. F., Fioletov, V. E., Dickerson, R. R., He, H., Lu, Z., and Streets, D. G.: Aura OMI observations of regional SO2 and NO2 pollution changes from 2005 to 2015, Atmos. Chem. Phys., 16, 4605–4629, https://doi.org/10.5194/acp-16-4605-2016, 2016.

Leitch, J. W., Delker, T., Good, W., Ruppert, L., Murcray, F., Chance, K., Liu, X., Nowlan, C., Janz, S., Krotkov, N., Pickering, E., Kowalewski, M., and J., W.: The GeoTASO airborne spectrometer project, Proc.SPIE, 9218, https://doi.org/10.1117/12.2063763, 2014.

Levelt, P., van den Oord, G., Dobber, M., Malkki, A., Visser, H., de Vries, J., Stammes, P., Lundell, J., and Saari, H.: The ozone monitoring instrument, IEEE T. Geosci. Remote., 44, https://doi.org/10.1109/TGRS.2006.872333, 2006.

lorga, G., Raicu, C. B., and Stefan, S.: Annual air pollution level of major primary pollutants in Greater Area of Bucharest, Atmospheric Pollution Research, 6, 824–834, https://doi.org/10.5094/APR.2015.091, 2015.

Lübcke, P., Bobrowski, N., Illing, S., Kern, C., Alvarez Nieves, J. M., Vogel, L., Zielcke, J., Delgado Granados, H., and Platt, U.: On the absolute calibration of SO_2 cameras, Atmospheric Measurement Techniques, 6, 677–696, https://doi.org/10.5194/amt-6-677-2013, 2013.

Ma, J. Z., Beirle, S., Jin, J. L., Shaiganfar, R., Yan, P., and Wagner, T.: Tropospheric NO_2 vertical column densities over Beijing: results of the first three years of ground-based MAX-DOAS measurements (2008-2011) and satellite validation, Atmos. Chem. Phys., 13, 1547–1567, https://doi.org/10.5194/acp-13-1547-2013, 2013.

Marmureanu, L., Deaconu, L., Vasilescu, J., Ajtai, N., and Talianu, C.: Combined optoelectronic methods used in the monitoring of SO_2 emissions and imissions, Environ. Eng. Manag. J., 12, 277–282, 2013.

Martin, R. V., Parrish, D. D., Ryerson, T. B., Nicks, J. K., Chance, K., Kurosu, T. P., Jacob, D. J., Sturges, E. D., Fried, A., and Wert, B. P.: Evaluation of GOME satellite measurements of tropospheric NO2 and HCHO using regional data from aircraft campaigns in the southeastern United States, Journal of Geophysical Research D: Atmospheres, https://doi.org/10.1029/2004JD004869, 2004.

Meier, A. C.: Measurements of horizontal trace gas distributions using airborne imaging differential optical absorption spectroscopy, Ph.D. thesis, University of Bremen, 2018.

Meier, A. C., Schönhardt, A., Bösch, T., Richter, A., Seyler, A., Ruhtz, T., Constantin, D.-E., Shaiganfar, R., Wagner, T., Merlaud, A., Van Roozendael, M., Belegante, L., Nicolae, D., Georgescu, L., and Burrows, J. P.: High-resolution airborne imaging DOAS measurements of NO_2 above Bucharest during AROMAT, Atmos. Meas. Tech., 10, 1831–1857, https://doi.org/10.5194/amt-10-1831-2017, 2017.

Merlaud, A.: Development and use of compact instruments for tropospheric investigations based on optical spectroscopy from mobile platforms, Presses univ. de Louvain, 2013.

Merlaud, A., Tack, F., Constantin, D., Georgescu, L., Maes, J., Fayt, C., Mingireanu, F., Schuettemeyer, D., Meier, A. C., Schönardt, A., Ruhtz, T., Bellegante, L., Nicolae, D., Den Hoed, M., Allaart, M., and Van Roozendael, M.: The Small Whiskbroom Imager for atmospheric compositioN monitorinG (SWING) and its operations from an unmanned aerial vehicle (UAV) during the AROMAT campaign, Atmos. Meas. Tech., 11, 551–567, https://doi.org/10.5194/amt-11-551-2018, 2018.

Nisulescu, C., Calinoiu, D., Timofte, A., Boscornea, A., and Talianu, C.: Diurnal Variation of Particulate Matter in the Proximity of Rovinari Fossil-Fuel Powerplant, Environ. Eng. Manag. J., 10, 99–105, 2011.

https://doi.org/10.5194/amt-2019-496
Preprint. Discussion started: 6 February 2020

Atmospheric Measurement Techniques Discussions

Nowlan, C. R., Liu, X., Leitch, J. W., Chance, K., González Abad, G., Liu, C., Zoogman, P., Cole, J., Delker, T., Good, W., Murcray, F., Ruppert, L., Soo, D., Follette-Cook, M. B., Janz, S. J., Kowalewski, M. G., Loughner, C. P., Pickering, K. E., Herman, J. R., Beaver, M. R., Long, R. W., Szykman, J. J., Judd, L. M., Kelley, P., Luke, W. T., Ren, X., and Al-Saadi, J. A.: Nitrogen dioxide observations from the Geostationary Trace gas and Aerosol Sensor Optimization (GeoTASO) airborne instrument: Retrieval algorithm and measurements during DISCOVER-AQ Texas 2013, Atmos. Meas. Tech., 9, 2647–2668, https://doi.org/10.5194/amt-9-2647-2016, 2016.

Nowlan, C. R., Liu, X., Janz, S. J., Kowalewski, M. G., Chance, K., Follette-Cook, M. B., Fried, A., González Abad, G., Herman, J. R., Judd, L. M., Kwon, H.-A., Loughner, C. P., Pickering, K. E., Richter, D., Spinei, E., Walega, J., Weibring, P., and Weinheimer, A. J.: Nitrogen dioxide and formaldehyde measurements from the GEOstationary Coastal and Air Pollution Events (GEO-CAPE) Airborne Simulator over Houston, Texas, Atmos. Meas. Tech., 11, 5941–5964, https://doi.org/10.5194/amt-11-5941-2018, 2018.

Parrish, D. D., Ryerson, T. B., Mellqvist, J., Johansson, J., Fried, A., Richter, D., Walega, J. G., Washenfelder, R. A., De Gouw, J. A., Peischl, J., Aikin, K. C., McKeen, S. A., Frost, G. J., Fehsenfeld, F. C., and Herndon, S. C.: Primary and secondary sources of formaldehyde in urban atmospheres: Houston Texas region, Atmos. Chem. Phys., 12, 3273–3288, https://doi.org/10.5194/acp-12-3273-2012, 2012.

Platt, U. and Stutz, J.: Differential Optical Absorption Spectroscopy: Principles and Applications, Physics of Earth and Space Environments, Springer, Berlin, 2008.

Richter, A., Richter, A., Weber, M., Burrows, J. P., Lambert, J.-C., and van Gijsel, A.: Validation strategy for satellite observations of tropospheric reactive gases, Annals of Geophysics, 56, https://doi.org/10.4401/ag-6335, 2014.

Schaub, D., Boersma, K. F., Kaiser, J. W., Weiss, A. K., Folini, D., Eskes, H. J., and Buchmann, B.: Comparison of GOME tropospheric NO2 columns with NO2 profiles deduced from ground-based in situ measurements, Atmos. Chem. Phys., 6, https://doi.org/10.5194/acp-6-3211-2006, 2006.

Schönhardt, A., Altube, P., Gerilowski, K., Krautwurst, S., Hartmann, J., Meier, A. C., Richter, A., and Burrows, J. P.: A wide field-of-view imaging DOAS instrument for two-dimensional trace gas mapping from aircraft, Atmos. Meas. Tech., 8, 5113–5131, https://doi.org/10.5194/amt-8-5113-2015, 2015.

Shaiganfar, R., Beirle, S., Denier van der Gon, H., Jonkers, S., Kuenen, J., Petetin, H., Zhang, Q., Beekmann, M., and Wagner, T.: Estimation of the Paris NO_x emissions from mobile MAX-DOAS observations and CHIMERE model simulations during the MEGAPOLI campaign using the closed integral method, Atmos. Chem. Phys., 17, 7853–7890, https://doi.org/10.5194/acp-17-7853-2017, 2017.

Sluis, W. W., Allaart, M. A. F., Piters, A. J. M., and Gast, L. F. L.: The development of a nitrogen dioxide sonde, Atmos. Meas. Tech., 3, 1753–1762, https://doi.org/10.5194/amt-3-1753-2010, 2010.

St. Clair, J. M., Swanson, A. K., Bailey, S. A., Wolfe, G. M., Marrero, J. E., Iraci, L. T., Hagopian, J. G., and Hanisco, T. F.: A new non-resonant laser-induced fluorescence instrument for the airborne in situ measurement of formaldehyde, Atmos. Meas. Tech., 10, 4833–4844, https://doi.org/10.5194/amt-10-4833-2017, 2017.

Stefan, S., Radu, C., and Belegante, L.: Analysis of air quality in two sites with different local conditions, Environ. Eng. Manag. J., 12, 371–379, 2013.

Tack, F., Merlaud, A., Meier, A. C., Vlemmix, T., Ruhtz, T., Iordache, M.-D., Ge, X., van der Wal, L., Schuettemeyer, D., Ardelean, M., Calcan, A., Constantin, D., Schönhardt, A., Meuleman, K., Richter, A., and Van Roozendael, M.: Intercomparison of four airborne imaging DOAS systems for tropospheric NO_2 mapping – the AROMAPEX campaign, Atmos. Meas. Tech., 12, 211–236, https://doi.org/10.5194/amt-12-211-2019, 2019.

Theys, N., Hedelt, P., De Smedt, I., Lerot, C., Yu, H., Vlietinck, J., Pedergnana, M., Arellano, S., Galle, B., Fernandez, D., Carlito, C. J., Barrington, C., Taisne, B., Delgado-Granados, H., Loyola, D., and Van Roozendael, M.: Global monitoring of volcanic SO 2 degassing

https://doi.org/10.5194/amt-2019-496
Preprint. Discussion started: 6 February 2020

with unprecedented resolution from TROPOMI onboard Sentinel-5 Precursor, Sci. Rep., 9, https://doi.org/10.1038/s41598-019-39279-y, 2019.

Timofte, A., Belegante, L., Cazacu, M. M., B., A., C., T., and S., G.: Study of planetary boundary layer height from LIDAR measurements and ALARO model, J. Optoelectron. Adv. M., 17, 2015.

Trombetti, M., Thunis, P., Bessagnet, B., Clappier, A., Couvidat, F., Guevara, M., Kuenen, J., and López-Aparicio, S.: Spatial inter-comparison of Top-down emission inventories in European urban areas, Atmos. Env., 173, 142–156, https://doi.org/10.1016/J.ATMOSENV.2017.10.032, 2018.

Veefkind, J., Aben, I., McMullan, K., Förster, H., de Vries, J., Otter, G., Claas, J., Eskes, H., de Haan, J., Kleipool, Q., van Weele, M., Hasekamp, O., Hoogeveen, R., Landgraf, J., Snel, R., Tol, P., Ingmann, P., Voors, R., Kruizinga, B., Vink, R., Visser, H., and Levelt, P.: TROPOMI on the ESA Sentinel-5 Precursor: A GMES mission for global observations of the atmospheric composition for climate, air quality and ozone layer applications, Remote Sens. Environ., 120, 70 – 83, https://doi.org/https://doi.org/10.1016/j.rse.2011.09.027, 2012.

von Clarmann, T.: Validation of remotely sensed profiles of atmospheric state variables: strategies and terminology, Atmos. Chem. Phys., 6, 4311–4320, https://doi.org/10.5194/acp-6-4311-2006, 2006.

Wagner, T., Ibrahim, O., Shaiganfar, R., and Platt, U.: Mobile MAX-DOAS observations of tropospheric trace gases, Atmos. Meas. Tech., 3, 129–140, 2010.

Wang, Y., Beirle, S., Lampel, J., Koukouli, M., De Smedt, I., Theys, N., Li, A., Wu, D., Xie, P., Liu, C., Van Roozendael, M., Stavrakou, T., Müller, J.-F., and Wagner, T.: Validation of OMI, GOME-2A and GOME-2B tropospheric NO2, SO2 and HCHO products using MAX-DOAS observations from 2011 to 2014 in Wuxi, China: investigation of the effects of priori profiles and aerosols on the satellite products, Atmos. Chem. Phys., 17, 5007–5033, https://doi.org/10.5194/acp-17-5007-2017, 2017.

https://doi.org/10.5194/amt-2019-496
Preprint. Discussion started: 6 February 2020

Atmospheric Measurement Techniques Discussions

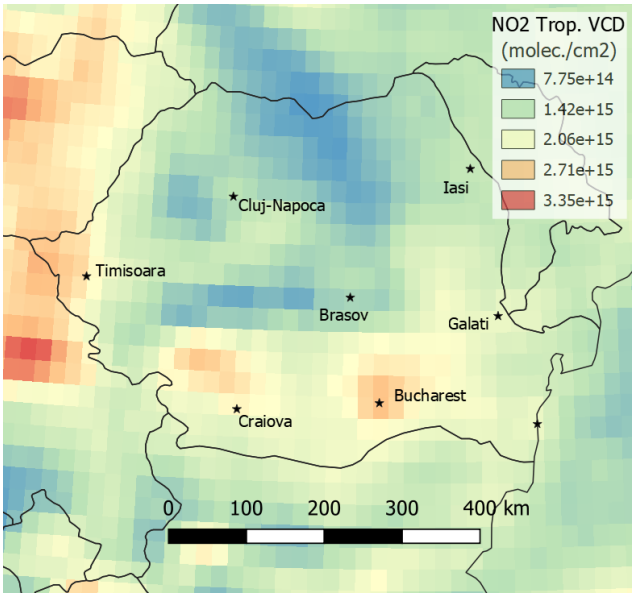

Figure 1. The tropospheric NO_2 VCD field seen from space with the OMI/AURA instrument above Romania (OMNO2d product, averaged for 2012-2016 with Giovanni, NASA GES DISC). The black stars pinpoint the largest cities of Romania.

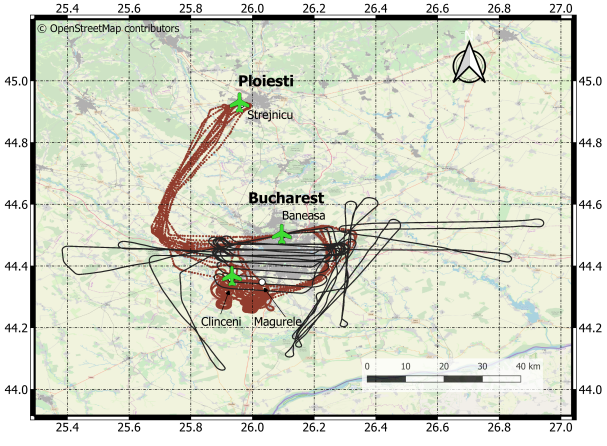

Figure 2. The Bucharest area with important locations for the AROMAT campaigns: the INOE atmospheric observatory in Magurele, the Baneasa airport, and the Clinceni airfield. Buit-up areas appear in grey. The red and black lines, respectively, show the BN-2 and Cessna flight tracks during AROMAT-2. © OpenStreetMap contributors 2019. Distributed under a Creative Commons BY-SA License.

https://doi.org/10.5194/amt-2019-496
Preprint. Discussion started: 6 February 2020

Atmospheric Measurement Techniques Discussions

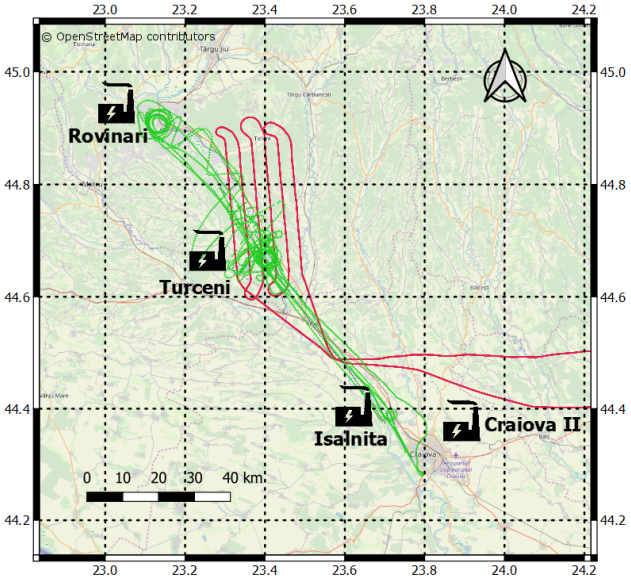

Figure 3. The Jiu Valley and its four power plants between Targu Jiu and Craiova. The scientific crew was based in Turceni during the AROMAT campaigns. The green and red lines, respectively, show the ultralight and Cessna flight tracks during AROMAT-2.
© OpenStreetMap contributors 2019. Distributed under a Creative Commons BY-SA License.

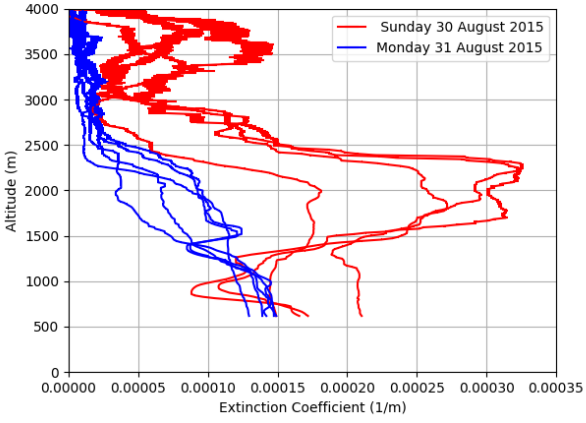

Figure 4. RALI extinction profiles at 532 nm above Magurele during two days of AROMAT-2. The different lines correspond to the different lidar measurements between 07:33 and 12:32 UTC (30 August 2015) and 07:29 and 15:01 UTC (31 August 2015).

https://doi.org/10.5194/amt-2019-496
Preprint. Discussion started: 6 February 2020

Atmospheric Measurement Techniques Discussions

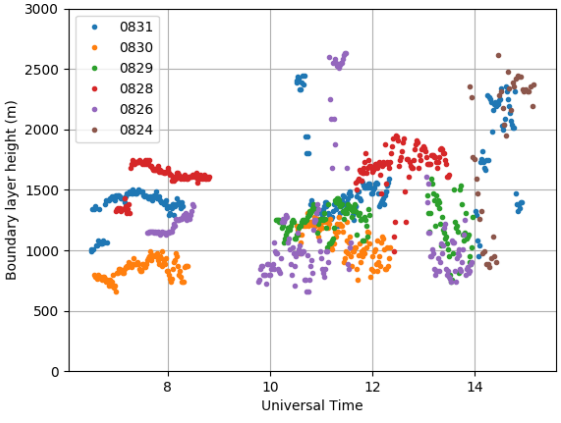

Figure 5. Lidar-derived boundary layer heights above Magurele in August 2015 during AROMAT-2.

https://doi.org/10.5194/amt-2019-496
Preprint. Discussion started: 6 February 2020

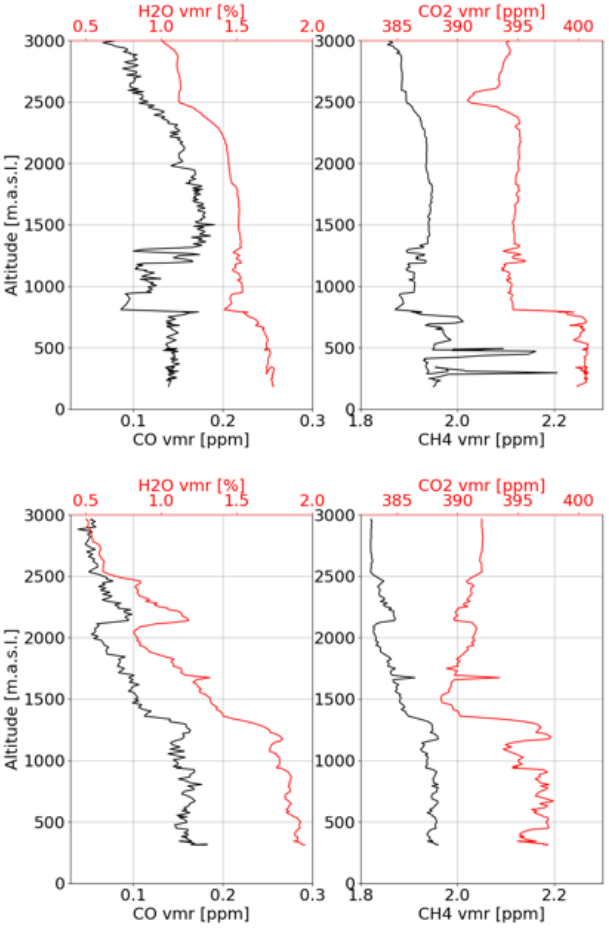

Figure 6. Vertical distributions of gases measured from the BN-2 during AROMAT-2 with the PICARRO. The upper panels shows the sounding at 08:30 UTC on 30 August 2015, the lower panel shows the sounding at 12:30 UTC on 31 August 2015.

https://doi.org/10.5194/amt-2019-496
Preprint. Discussion started: 6 February 2020

Atmospheric Measurement Techniques Discussions

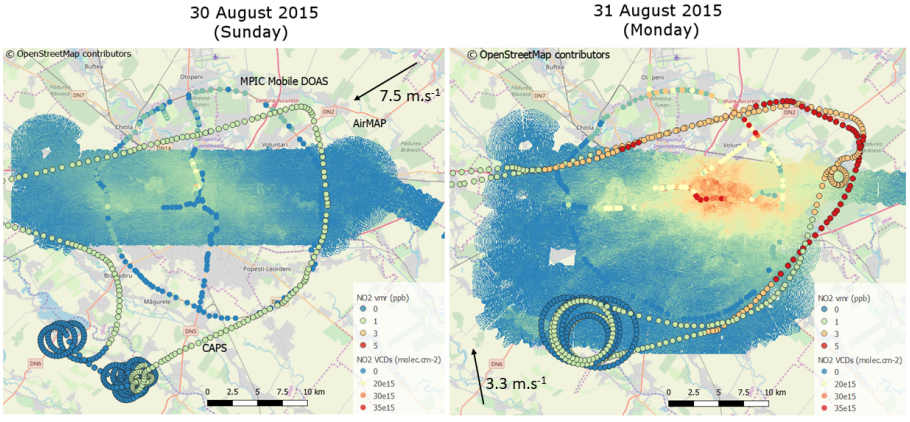

Figure 7. Measurements of NO_2 VCDs and volume mixing ratios in Bucharest on 30 (Sunday) and 31 (Monday) August 2015 with AirMAP (continuous map), the CAPS (black-rimmed circles), and the MPIC Mobile-DOAS (plain colour circles). © OpenStreetMap contributors 2019. Distributed under a Creative Commons BY-SA License.

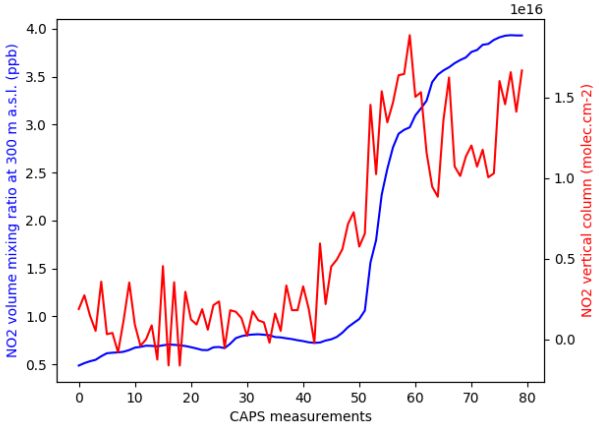

Figure 8. Volume mixing ratio and VCDs of NO_2 in and out of the pollution plume of Bucharest, as measured with the CAPS (on the BN-2) and AirMAP (on the Cessna) during the afternoon flights on 31 August 2015. Note that the two measurements are not exactly time coincident and that the plot shows the VCDs extracted at the position of the CAPS measurements.

https://doi.org/10.5194/amt-2019-496
Preprint. Discussion started: 6 February 2020

Atmospheric Measurement Techniques Discussions

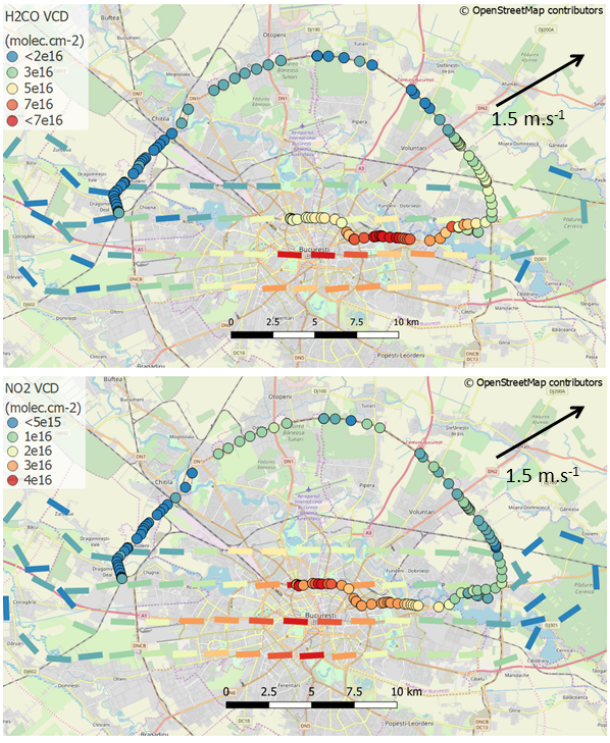

Figure 9. Horizontal distribution of tropospheric H_2CO and NO_2 VCDs measured on 31 August 2015 with the IUP-UB nadir-only compact spectrometer from the Cessna (flight tracks) and with the MPIC Mobile-DOAS (coloured circles). © OpenStreetMap contributors 2019. Distributed under a Creative Commons BY-SA License.

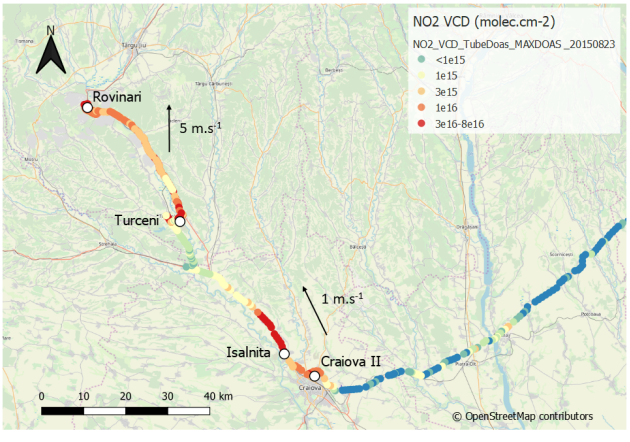

Figure 10. Tropopsheric vertical column densities of NO_2 measured with the MPIC Mobile-DOAS instruments in the Jiu Valley on 23 August 2015. © OpenStreetMap contributors 2019. Distributed under a Creative Commons BY-SA License.

https://doi.org/10.5194/amt-2019-496
Preprint. Discussion started: 6 February 2020

Atmospheric Measurement Techniques Discussions

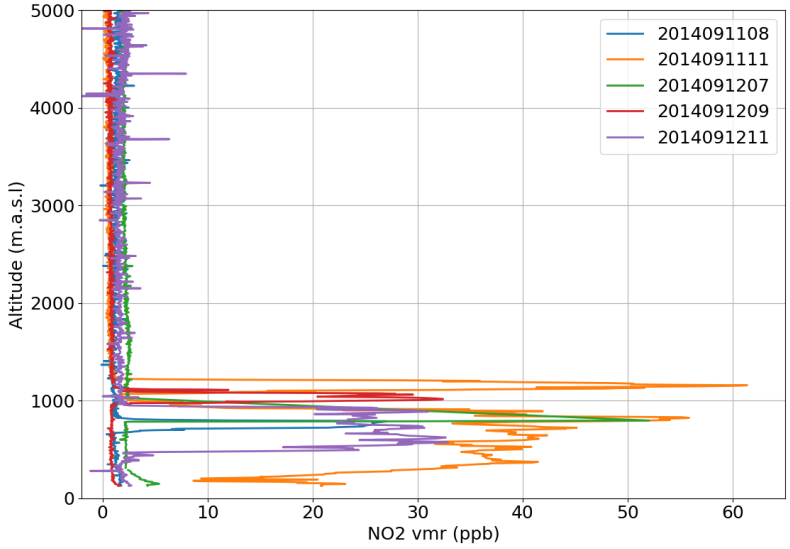

Figure 11. Examples of NO_2 sondes data from Turceni during AROMAT-1 (11 and 12 September 2014).

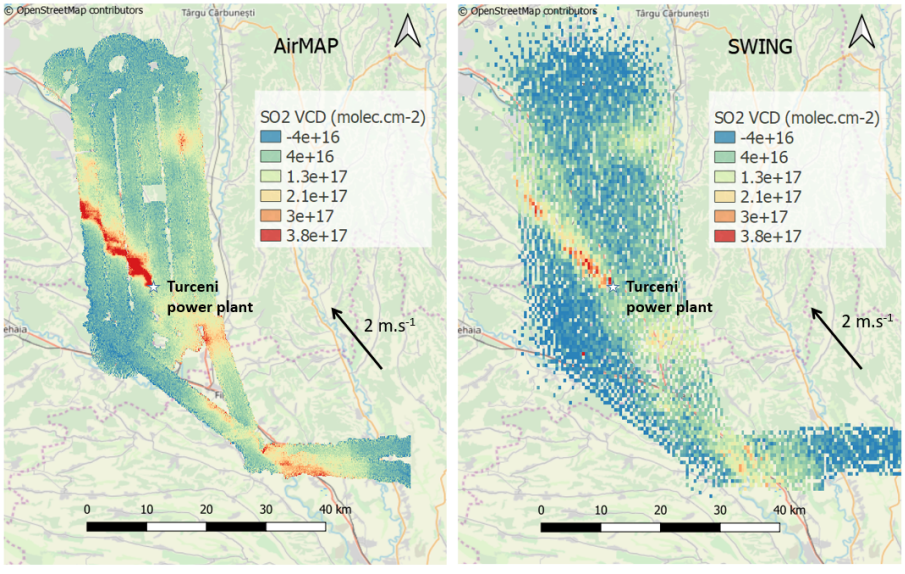

Figure 12. AirMAP (left panel) and SWING (right panel) measurements of SO_2 from the Cessna above the Jiu Valley on 28 August 2015. © OpenStreetMap contributors 2019. Distributed under a Creative Commons BY-SA License.

https://doi.org/10.5194/amt-2019-496
Preprint. Discussion started: 6 February 2020

Atmospheric Measurement Techniques Discussions

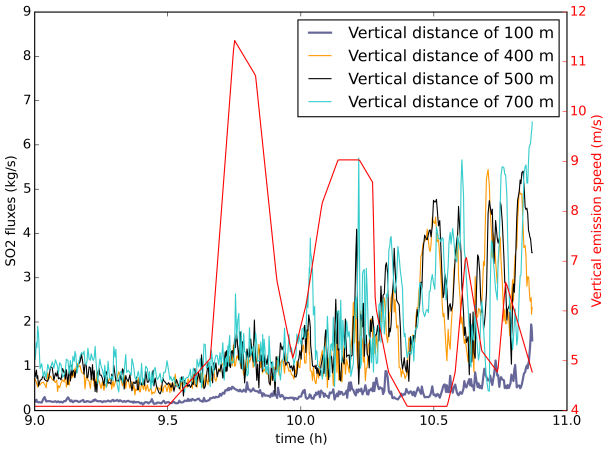

Figure 13. SO_2 fluxes from the Turceni power plant on 28 August 2015. They were estimated with the Envicam2 SO_2 camera for 4 transverses at vertical altitudes above the stack of 100, 400, 500 and 700 m. The red line shows the estimated plume speed ($m.s^{-1}$).

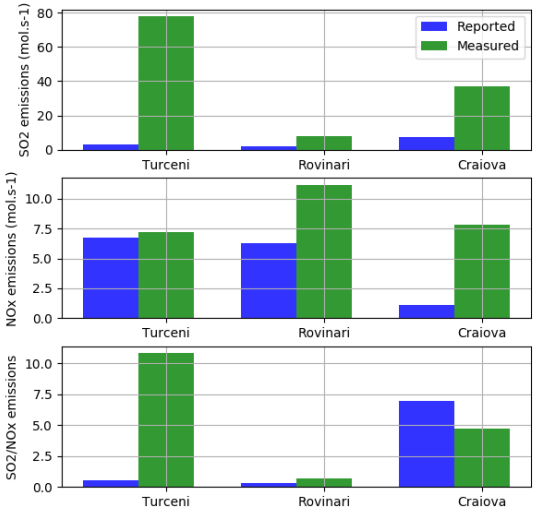

Figure 14. SO_2 and NO_x fluxes from three power plants of the Jiu Valley as (1) measured with the ULMDOAS on 26 August 2015 (green bars) and (2) estimated from the reported emissions of 2015 assuming constant emissions throughout the year (blue bars). Uncertainties on the ULMDOAS-derived fluxes are around 60%.

https://doi.org/10.5194/amt-2019-496
Preprint. Discussion started: 6 February 2020

Atmospheric Measurement Techniques Discussions

Table 1. Past and near-future space missions focused on air quality: coverage, pixel size, and temporal sampling.

Launch year	Instrument	Pixel size at nadir (km^2)	Coverage	Revisit time
1995	GOME	320 x 40	Global	3 days
2002	SCIAMACHY	60 x 30	Global	6 days
2004	OMI	13 x 24	Global	1 day
2006	GOME-2	80 x 40	Global	1 day
2011	OMPS	50 x 50	Global	1 day
2017	TROPOMI	3.5 x 5.5	Global	1 day
2023 (planned)	Sentinel-5	7 x 7	Global	1 day
2020 (planned)	GEMS	7 x 8	East Asia	1 hour
2022 (planned)	TEMPO	2 x 4.5	North America	1 hour
2023 (planned)	Sentinel-4	8 x 8	Europe	1 hour

Table 2. Data quality targets for the S5P TROPOMI data products relevant in the AROMAT context (extracted from ESA (2014)).

Product	Accuracy	Precision
Tropospheric NO_2	25-50%	$7x10^{14}$ molec cm^{-2}
Tropospheric SO_2	30-50%	$2.7\text{-}8.1x10^{16}$ molec cm^{-2}
Total H_2CO	40-80%	$0.4\text{-}1.2x10^{16}$ molec cm^{-2}

Table 3. Main characteristics of the power plants of the Jiu Valley.

	Craiova II	Islanita	Turceni	Rovinari
Latitude (°N)	44.343	44.39	44.67	44.91
Longitude (°E)	23.81	23.72	23.41	23.135
Nominal capacity (MW)	300	630	1650	1320
Smokestack height (m)	149	200	280	280

https://doi.org/10.5194/amt-2019-496
Preprint. Discussion started: 6 February 2020

Atmospheric Measurement Techniques Discussions

Table 4. Summary of the AROMAT measurements of NO_2.

Instrument	Type	Ground Sampling Distance (m)	Observed range (molec cm^{-2} / ppb)	Detection limit (molec cm^{-2} / ppb)	Bias (%)	Reference
AirMAP	Imager	100	0-8 x 10^{16}	1.5 x 10^{15}	25%	Meier et al. (2017)
SWING	Imager	300	0-8 x 10^{16}	1.2 x 10^{15}	25%	Merlaud et al. (2018)
ULMDOAS	Nadir	400	0-1.7 x 10^{17}	5 x 10^{14}	25%	Constantin et al. (2017)
Tube MAX-DOAS	car-based	500	0-1.3 x 10^{17}	1.3 x 10^{14}	20%	Donner et al. (2015)
Mini Max-DOAS	car-based	500	0-1.3 x 10^{17}	6 x 10^{14}	20%	Wagner et al. (2010)
UGAL Mobile	car-based	500	0-2.5 x 10^{17}	4 x 10^{14}	25%	Constantin et al. (2013)
BIRA Mobile	car-based	500	0-1.3 x 10^{17}	8 x 10^{14}	20%	Merlaud (2013)
KNMI sonde	in-situ	n.a.	0-60	1	40%	Sluis et al. (2010)
CAPS	in-situ	n.a.	0-20	0.1	40%	Kebabian et al. (2005)

Table 5. Summary of the AROMAT measurements of H_2CO.

Instrument	Type	Ground Sampling Distance (m)	Observed range (molec cm^{-2})	Detection limit (molec cm^{-2})	Bias (%)	Reference
Bremen nadir	Airborne nadir	1800	1-7 x 10^{16}	6 x 10^{15}	25%	Bösch et al. (2016)
Tube MAX-DOAS	car-based	500	1-7.5 x 10^{16}	8 x 10^{14}	20%	Donner et al. (2015)

Table 6. Summary of the AROMAT measurements of SO_2.

Instrument	Type	Ground Sampling Distance (m)	Observed range (molec cm^{-2})	Detection limit (molec cm^{-2})	Bias (%)	Reference
AirMAP	Imager	100	0-6 x 10^{17}	1.7 x 10^{16}	40%	Meier et al. (2017)
SWING	Imager	300	0-4 x 10^{17}	2 x 10^{16}	40%	Merlaud et al. (2018)
ULMDOAS	Nadir	400	0-2.5x 10^{18}	3 x 10^{15}	40%	Constantin et al. (2017)
Tube MAX-DOAS	car-based	500	0-1x10^{18}	5 x 10^{15}	20%	Donner et al. (2015)
Mini Max-DOAS	car-based	500	0-2.2x10^{18}	1 x 10^{16}	20%	Wagner et al. (2010)
UGAL Mobile	car-based	500	0-4x 10^{18}	4 x 10^{15}	25%	Constantin et al. (2013)

https://doi.org/10.5194/amt-2019-496
Preprint. Discussion started: 6 February 2020

Atmospheric Measurement Techniques Discussions

Table 7. Total simulated error budget for the validation of spaceborne NO_2 VCDs validation using airborne mapping at different resolution, with or without profile informations.

		Precision (molec cm^{-2})			Accuracy		
	Place	Shot noise	Time error	Tot.	Ref.	Fit	Tot.
AirMAP	B	$3x10^{13}$	$4x10^{15}$	$4.1x10^{15}$	26%	6%	37%
SWING	B	$7x10^{13}$	$4x10^{15}$	$4.1x10^{15}$	26%	6%	37%
AirMAP + profile	B	$3x10^{13}$	$4x10^{15}$	$4.1x10^{15}$	10%	6%	28%
AirMAP	T	$3x10^{13}$	$4x10^{15}$	$4.1x10^{15}$	26%	10%	37%
AirMAP + profile	T	$3x10^{13}$	$4x10^{15}$	$4.1x10^{15}$	10%	10%	29%

Table 8. NO_x emissions from Bucharest estimated from the AROMAT measurements.

	AirMAP	Mobile-DOAS
8 September 2014	14.6 $mol.s^{-1}$	12.5 $mol.s^{-1}$
9 September 2014	13.1 $mol.s^{-1}$	n.a.
31 August 2015	n.a.	17.5 $mol.s^{-1}$

Table 9. NO_x and SO_2 emissions from the Turceni power plant estimated from the AROMAT measurements.

	Instrument	Distance	SO_2 flux	NO_x flux	$\frac{SO_2}{NO_2}$
11 September 2014 - 09:00 UTC	AirMAP	7 km	n.a.	8 $mol.s^{-1}$	n.a.
25 August 2015 - 07:45 UTC	Mobile-DOAS	1 km	105 $mol.s^{-1}$	4 $mol.s^{-1}$	15.4
25 August 2015 - 08:30 UTC	Mobile-DOAS	1 km	52 $mol.s^{-1}$	2 $mol.s^{-1}$	26
25 August 2015 - 08:30 UTC	ULMDOAS	10 km	85 $mol.s^{-1}$	10 $mol.s^{-1}$	8.5
26 August 2015 - 10:00 UTC	ULMDOAS	5 km	78 $mol.s^{-1}$	6 $mol.s^{-1}$	13
27 August 2015 - 07:45 UTC	ULMDOAS	8.5 km	145 $mol.s^{-1}$	17 $mol.s^{-1}$	8.5
27 August 2015 - 07:55 UTC	Mobile-DOAS	1 km	77 $mol.s^{-1}$	5 $mol.s^{-1}$	16
28 August 2015 - 07:00 UTC	Mobile-DOAS	1 km	24.8 $mol.s^{-1}$	1.7 $mol.s^{-1}$	14.7
28 August 2015 - 10:00 UTC	AirMAP	7 km	25 $mol.s^{-1}$	8 $mol.s^{-1}$	3.1
28 August 2015 - 10:15 UTC	Mobile-DOAS	1 km	32 $mol.s^{-1}$	4 $mol.s^{-1}$	8
28 August 2015 - 09:00-11:00 UTC	SO_2 camera	Above stack	15.6-62.4 $mol.s^{-1}$	n.a	n.a.